Research Square

Preprints are preliminary reports that have not undergone peer review.
They should not be considered conclusive, used to inform clinical practice,
or referenced by the media as validated information.

Fabrication of Rice Husk Biochar under Varying Pyrolysis Conditions for Soil Amendment and Enhanced Agronomic Traits of Wheat (Triticum aestivum L.)

Sri Abisankar. M
Karunya Institute of Technology and Sciences
Augustine R
augustinerajendran@gmail.com
Karunya Institute of Technology and Sciences
Stefano Amaducci
Università Cattolica del Sacro Cuore
Vikas V K
ICAR-Indian Agricultural Research Institute, Regional Station, Wellington, India
Ramesh Kumar P
Karunya Institute of Technology and Sciences
Praveena Katharine S
Karunya Institute of Technology and Sciences
Indira Petchiammal K
Karunya Institute of Technology and Sciences

Article

Keywords: Crop growth, Physicochemical characterization, Pyrolysis temperature, Rice husk biochar, Wheat, and yield.

Posted Date: November 24th, 2026

DOI: https://doi.org/10.21203/rs.3.rs-11814557/v1

License: This work is licensed under a Creative Commons Attribution 4.0 International License.
Read Full License

Additional Declarations: No competing interests reported.

Fabrication of Rice Husk Biochar under Varying Pyrolysis Conditions for Soil Amendment and Enhanced Agronomic Traits of Wheat (*Triticum aestivum* L.)

Sri Abisankar. M[1], Augustine. R[1*], Stefano Amaducci[2], Vikas. V.K.[3], Ramesh Kumar. P[4] Praveena Katharine. S[5], Indira Petchiammal. K[6].

[1]Division of Agronomy, School of Agricultural Sciences, Karunya Institute of Technology and Sciences, Coimbatore, Tamil Nadu. India.
[2]Department of Sustainable Crop Production, Università Cattolica del Sacro Cuore, via Emilia Parmense, 84, Piacenza, Italy.
[3]ICAR-Indian Agricultural Research Institute, Regional Station, Wellington, Ooty, Tamil Nadu, India.
[4]Division of Crop Physiology and Biochemistry, School of Agricultural Sciences, Karunya Institute of Technology and Sciences, Coimbatore, Tamil Nadu. India.
[5]Division of Soil Science, School of Agricultural Sciences, Karunya Institute of Technology and Sciences, Coimbatore, Tamil Nadu. India.
[6]Division of Genetics and Plant Breeding, School of Agricultural Sciences, Karunya Institute of Technology and Sciences, Coimbatore, Tamil Nadu, India
[*]Corresponding Author: augustinerajendran@gmail.com

Abstract

Rice husk, an abundant agricultural residue that is mostly wasted or burned, has potential as a biochar feedstock. This study examined how pyrolysis temperature affects the physicochemical and structural properties of rice husk biochar (RHB), and how RHB influences the germination, growth, and yield of wheat (*Triticum aestivum* L.). RHB was produced by slow pyrolysis at 250, 350, and 450 °C for 2 h. It was characterized in terms of proximate and chemical properties, morphology, elemental composition, and structure using SEM, EDAX, and XRD. Pot experiments assessed wheat germination, early seedling development, growth, and yield under control and RHB treatments. As pyrolysis temperature increased, biochar yield fell from about 69% at 250 °C to 40% at 450 °C. Moisture content also decreased, while ash and fixed carbon contents rose. RHB improved early seedling development, and the 450 °C biochar produced the fastest shoot and root growth. The 450 °C treatment also gave the greatest plant height, leaf number, dry weight, and leaf area index. It produced the most spikes and spikelets and the highest grain and stover yields. Pyrolysis temperature therefore markedly changed RHB properties, and these changes shaped wheat establishment, growth, and yield. Temperature-optimized RHB is a promising way to recycle residue for sustainable wheat production and agricultural waste management.

Keywords:

Crop growth, Physicochemical characterization, Pyrolysis temperature, Rice husk biochar, , Wheat, and yield.

Introduction

India is a country with agriculture as its core industry. After grain harvesting each year, the total volume of all types of crop residues left in the fields exceeds 500 million tons. Among these residues, the leftover stalks from rice, wheat, cotton, corn, millet, sugarcane, jute, rapeseed and mustard, and peanuts are almost always burned by farmers in situ on their own farmlands in rural areas across all Indian states[1]. The main reason such a large volume of crop residues is burned is that most of them have not found alternative uses, and burning is the most straightforward disposal method. But simply, it is to clear away the broken straw and piercing stubble left in the fields after harvest, to free up the land for the next round of planting before the sowing window for the next crop cycle arrives[2].

Crop residue burning is widespread in irrigated rice-growing regions, particularly where mechanized planting and harvesting are practiced. The practice of stubble burning, referred to as Parali burning in India, is the intentional act of setting fire to the leftover residues after crops have been harvested [3]. These practices generate large quantities of residues that are difficult to manage. Consequently, farmers often resort to open burning, causing environmental pollution[4]. Firstly, there is a shortage of labour there are not enough workers to process these residues. Second, the cost of clearing all the residues from the fields is too high, and the math never works out to be cost-effective. On top of that, more and more farmers now use combine harvesters to gather their crops[5]. The other issue humanity faces is the increasing demand for food by the world's population. As a result, there has been an increase in the amount of agricultural waste produced[6]. The most common method of disposing of such waste is through incineration. However, incinerating such waste poses a threat to the environment and human health[7]. Agricultural waste biomass can be converted into valuable products and energy. Its use in composite materials can reduce waste disposal and promote recycling and resource conservation[8].

Asia is the leading contributor to global biomass burning, accounting for 34% of the total, while India accounts for 18% of open burning in Asian countries[9]. According to the Ministry of New and Renewable Energy (MNRE), Government of India, the average annual crop residue production is 50 crore tons, with 9.2 crore tons burned and 14 crore tons remaining as surplus[10]. The Indian Agricultural Research Institute (IARI) in New Delhi has reported that cereal crops yield the highest amount of crop residue, totalling 35.2 crore tons, with paddy contributing 34% and wheat contributing 22%[11].

The loss of soil fertility and agricultural productivity due to low precipitation, soil salinity, nutrient leaching, and poor agricultural practices has spurred interest in developing sustainable management strategies for nutrient-poor soils to enhance crop sustainability[12]. In general, increasing crop productivity will lead to sustainable improvements in farmland, and enriching the soil fertility of existing agricultural land could also be a viable option[13]. Therefore, it seems that the application of biochar (with inherent mineral constituents) to nutrient-poor soils could be a potential means to enhance agricultural productivity[14]. Plant residue biochar, an alternative organic supplement to chemical fertilizers, could be a viable and sustainable means of enhancing crop yields[15] in degraded, nutrient-poor soils[16]. For a long time, people have been interested in using biochar derived from plant residues as a soil conditioner to enhance soil physicochemical properties and crop productivity[17]. The use of biochar in

agriculture as a potential means to enhance soil fertility can mitigate the adverse impacts of chemicalization on soil fertility[18], soil microbial biodiversity[19], and agricultural productivity[15].

Rice (*Oryza sativa*) is a major staple cereal widely consumed across Asia and Africa, providing substantial nutritional and caloric value due to its starch, protein, and fibre content. Rice husk, the major by-product of rice milling, is generated during the husking of paddy rice. Typically, the milling process yields about 0.28 kg of rice husk for every kg of milled white rice [20]. Rice husk is a major agricultural residue generated globally, with considerable potential for biochar production and carbon sequestration. Its global distribution is presented in **Fig. 1**. Rice husk is considered an agricultural residue coming from the rice industry. The lignocellulosic composition of rice husk depends on various factors, including agronomic management, weather conditions, and soil type[21]. The reported lignocellulosic composition of rice husk is cellulose 35%, hemicellulose 30%, lignin 18%, silica 13%, and miscellaneous components up to 4%[22]. Around 140 million tonnes of rice husk are generated annually worldwide, but are not properly utilized. This large amount of rice husk is either discarded or burnt in open fields, which is environmentally hazardous[23]. Rice husk, an agricultural by-product, is an essential raw material for producing biochar; however, pyrolysis temperature affects the physicochemical properties of rice husk and its interactions with plants and soil environment[24].

Biochar has higher nutrient retention capacity and greater resistance to microbial degradation, owing to its chemical and colloidal structure[25]. Despite significant nutrient losses during pyrolysis, biochar has positive effects on soil by neutralizing toxins and improving soil physical properties[26]. Increasing pyrolysis temperature alters biochar properties, including pH, surface area, porosity, ash content, nutrient composition, and functional groups, thereby affecting nutrient availability and plant growth[27]. Traditionally, rice husks are disposed of in landfills or burned at rice production sites, causing environmental concerns. However, rice husks can be recycled as a high-value carbon feedstock, offering a sustainable alternative for waste management and resource recovery[28]. Thus, recycling crop residues into high-value products is paramount for the sustainable management of agriculture. Converting biomass into biochar improves carbon sequestration in soil and mitigates climate change[29]. Biochar can support zero-waste agriculture by recycling crop residues and reducing environmental pollution. Optimizing its physicochemical properties and pyrolysis conditions is essential for effective soil management[30].

Wheat (*Triticum aestivum* L.) is one of the most significant cereal crops on the planet and is critical for food security worldwide; nevertheless, its productivity is affected by soil quality, access to water, and the efficiency of nutrient utilization early in the life cycle[31]. Recently, biochar has become popular as a sustainable soil amendment because of its high porosity, surface area, carbon stabilization, and potential to improve soil physicochemical properties, nutrient availability, plant growth, and water retention[32].

The present investigation analyzed how different pyrolysis temperatures (250, 350, and 450°C) of rice husk biochar (RHB) affect the growth and yield of wheat[33]. The present study aims to produce RHB at three pyrolysis temperatures (250 °C, 350 °C, and 450 °C) and to characterize the resulting biochars through physicochemical and structural analyses to understand how pyrolysis temperature shapes their properties. Building on this

characterization, the study further seeks to evaluate the effects of these biochars on wheat seed germination, vegetative growth, and yield performance under controlled pot experimental conditions. By comparing wheat responses across the three biochar treatments, the study aims to determine whether biochar production conditions effectively enhance overall crop growth and productivity, thereby linking these conditions to their agronomic value[34].

This assessment highlights how pyrolysis conditions influence biochar's agronomic performance and support the development of RHB based strategies to improve early crop growth and promote sustainable agriculture[35]. Therefore, appropriate management of crop residues for agricultural use is of great significance. Recent research efforts have developed conservation agriculture-based crop management technologies that are more resource-efficient than conventional practices.

The effects of RHB on soil nutrient status and crop productivity in nutrient-poor soils remain poorly understood. Therefore, this study evaluates the potential of RHB to improve soil conditions and enhance crop productivity.

Results

Influence of Pyrolysis Temperature on Biochar Yield

Fig. 3. The relationship between biochar yield and pyrolysis temperature was evaluated using linear and quadratic regression models. Biochar yield decreased from 69% at 250 °C to 45% at 350 °C, then to 40% at 450 °C, indicating a negative relationship between pyrolysis temperature and biochar yield. This decreasing trend indicates that increasing pyrolysis temperature promotes the release of moisture, volatile compounds, and low-molecular-weight gaseous products, thereby reducing the final biochar mass. Overall, biochar yield exhibited a negative relationship with pyrolysis temperature over the investigated temperature range (250–450 °C).

$$y = 2.05 - 0.77x + 8.89 \times 10^{-4}x^2 \quad (1)$$

Here, y denotes biochar yield (%) and x denotes pyrolysis temperature (°C). The quadratic fit captured the curvature of the data, showing a sharper decrease in yield from 250 to 350°C than from 350 to 450°C. It indicates that the rate of mass loss declines at higher temperatures as thermally reactive components of biomass are exhausted.

Proximate Analysis of Rice Husk Biochar

The proximal makeup of RHB generated at 250, 350, and 450°C was studied based on moisture, ash, volatile matter, and fixed carbon levels **Fig. 4(a-d)**. Significant changes were observed across all four indicators: as temperature increased, moisture decreased, while ash, volatile matter, and fixed carbon increased. Moisture content decreased progressively from approximately 7.5% at 250°C to 5.4% at 350°C and 3.5% at 450°C **Fig. 4(a)**, with the lowest value recorded at 450°C and the highest at 250°C. Ash content showed the opposite trend **Fig. 4(b)**, rising from approximately 28% at 250°C to 35% at 350°C and 48% at 450°C. The 450°C biochar therefore had the highest ash content, while the lowest was recorded at 250°C. Volatile matter also increased with temperature **Fig. 4(c)**, from approximately 24% at 250°C to 30% at 350°C and 36% at 450°C, with the highest value observed at 450°C. Similarly, fixed carbon content increased progressively with increasing pyrolysis temperature **Fig. 4(d)**. The fixed

carbon content increased from approximately 36% at 250°C to 40% at 350°C, then to approximately 44% at 450°C. Among the treatments, the biochar produced at 450°C had the highest fixed carbon content, whereas the 250°C treatment had the lowest.

Surface Morphology of Rice Husk Biochar at Varying Pyrolysis Temperatures

SEM micrographs in **Fig. 5(a-c)** revealed differences in the surface morphology and pore architecture of RHB produced at 250, 350, and 450°C, respectively. At 250°C **Fig. 5(a),** the surface was relatively compact and irregular, with shallow pores (Pa1 = 5.498 µm, Pa2 = 5.037 µm). At 350°C **Fig. 5(b)**, the structure was more distinctly porous with clearly visible cavities (Pa1 = 7.403 µm, Pa2 = 3.954 µm). At 450°C **Fig. 5(c)**, the surface showed well-defined open pores along with relatively smoother regions (Pa1 = 3.875 µm, Pa2 = 4.405 µm). Overall, surface morphology and pore features varied among the biochar produced at the three pyrolysis temperatures.

Grey Level (GL) Intensity Mapping and Pore Distribution

The grey-level (GL) intensity maps in **Fig. 5(d-f)** showed variations in surface intensity among the biochars, with the colour scale ranging from low-intensity blue/violet regions (GL ≈ 0-50) to high-intensity yellow/orange/white regions (GL ≈ 150-250). At 250°C **Fig. 5(d)**, the map was dominated by blue and green tones with scattered green-yellow regions. At 350°C **Fig. 5 (e)**, yellow-to-orange regions were more prominent around surface features and pores, showing greater intensity variation. At 450°C **Fig. 5(f)**, pronounced orange-to-white regions appeared, including areas with GL values above 200, together with distinct blue regions. Overall, the spatial distribution and intensity of surface features differed clearly among the three pyrolysis temperatures.

Elemental Composition via EDAX Analysis

Energy-dispersive X-ray (EDAX) analysis of selected regions (Spectrum 1) of RHB produced at 250, 350, and 450°C, along with the corresponding SEM micrographs and spectra, is shown in **Fig. 6(a-f)**. At 250°C **Fig. 6(a, d)**, the surface had pronounced globular, blister-like protrusions, and the spectrum showed a strong silicon (Si) peak, a moderate oxygen (O) peak, and a minor carbon (C) signal. At 350°C **Fig. 6(b, e)**, the surface had irregular, angular particulate fragments, and the spectrum was dominated by C, followed by O and Si, with a trace molybdenum (Mo) signal. At 450°C **Fig. 6(c, f)**, numerous small angular mineral/char fragments lay over a granular background, and the spectrum was similar to that at 350°C, with a minor additional peak near 3-3.5 keV and low background counts (Full-Scale value of 1241 counts).

X-ray Diffraction (XRD) Analysis

The XRD patterns of RHB produced at 250, 350, and 450°C are shown in **Fig. 7** (curves vertically offset for clarity). All three samples showed a broad, diffuse hump centred around $2\theta \approx 20\text{-}25°$. At 250°C (curve a), the hump had relatively high baseline noise, with weak, poorly resolved reflections near $2\theta \approx 44°$, 65°, and 78°. At 350°C (curve b), the hump was more clearly defined, and the reflections were sharper and better resolved. At 450°C (curve c), the hump

was retained, and the reflections remained sharp, with the peak near 78° showing comparatively higher intensity, while the region below $2\theta < 15°$ had an elevated, less structured baseline.

Influence of Pyrolysis Temperature on Wheat Seed Germination and Early Seedling Morphological Development

The visual response of wheat seedlings to RHB produced at different pyrolysis temperatures is presented in **Fig. 8 (a–h).** In the control treatment **Fig. 8(a)**, the germinated seeds exhibited shoot emergence and root development, with visible variations in seedling growth. The corresponding individual seedling **Fig. 8(e)** showed shoot elongation accompanied by a prominent primary root and limited lateral root development. In the 250 °C biochar treatment **Fig. 8(b)**, seedlings exhibited visible shoot emergence and root development across the Petri dish. The individual seedling **Fig. 8(f)** showed shoot elongation along with an extended primary root and the development of lateral roots. In the 350 °C biochar treatment **Fig. 8(c)**, germination and seedling establishment were also observed, with emerging shoots and developing root systems. The corresponding individual seedling **Fig. 8(g)** displayed shoot elongation and an elongated root system with visible branching.

Modulation of Wheat Seed Germination and Seedling Growth by Rice Husk Biochar Produced at Different Pyrolysis Temperatures

The effects of RHB produced at different pyrolysis temperatures on wheat germination and early seedling growth are presented in **Fig. 9.** Visual observations **Fig. 9(a)** revealed variations in shoot development and root architecture among the treatments. Biochar-amended seedlings exhibited visible improvements in shoot elongation and root development compared with the control. The quantitative results **Fig. 9(b)** showed that germination percentage progressively increased from 85% in the control to 87%, 91%, and 95% under the 250, 350, and 450 °C treatments, respectively. Similarly, shoot length, root length, and total seedling length showed increasing trends with increasing biochar pyrolysis temperature, with the highest values observed under the 450 °C treatment. The root-to-shoot ratio also varied among the treatments. Overall, RHB produced at 450 °C exhibited the most favourable response in terms of wheat germination and early seedling growth.

Growth Performance of Wheat Plants under Different Rice Husk Biochar Treatments

The overall growth performance of wheat plants under different RHB treatments is presented in **Fig. 10**. The control plants **Fig. 10(a)** exhibited comparatively limited plant growth and spike development. Biochar-amended plants showed visible variations in plant height, tillering, and spike formation. The 250 °C treatment **Fig. 10(b)** showed improved vegetative growth, while the 350 °C treatment **Fig. 10(c)** exhibited well-developed shoots and spike formation. Similarly, plants treated with 450 °C biochar **Fig. 10(d)** displayed vigorous vegetative growth with visible tiller development and spike formation. Overall, the representative images indicate differences in wheat growth performance among the biochar treatments, with comparatively better visual growth observed under the higher-temperature biochar treatments.

Wheat Growth Traits Under Different Rice Husk Biochar Pyrolysis Temperatures

RHB application clearly improved plant growth, with the highest values consistently recorded under the 450°C treatment **Fig. 11**. Plant height reached a maximum of 86.59 cm **Fig. 11(a)**, the number of leaves increased to 11 leaves plant^{-1} **Fig. 11(b)**, dry matter production was highest at 42 g pot^{-1} **Fig. 11(c)**, and the leaf area index (LAI) peaked at 7.0 **Fig. 11(d)**. The 450°C treatment exceeded the other RHB treatments for all parameters **Fig. 11(a-d)**, with the increase particularly evident in dry matter production and LAI **Fig. 11(c-d)**, indicating greater biomass accumulation and leaf area development.

Wheat Yield Traits Under Different Rice Husk Biochar Pyrolysis Temperatures

RHB application significantly influenced the yield attributes and yield of wheat, with the highest values consistently recorded under the 450°C treatment **Fig. 12**. The number of spikes increased from 35 spikes plant^{-1} in the control to 48 under 450°C RHB **Fig. 12(a)**, and spikelets reached a maximum of 21 spikelets spike^{-1} compared with 12 in the control **Fig. 12(b)**. Grain yield rose progressively with pyrolysis temperature, from 12 g pot^{-1} in the control to 21 g pot^{-1} under 450 °C **Fig. 12(c)**, and stover yield increased from 24 to 32 g pot^{-1} **Fig. 12(d)**. Higher-temperature RHB treatments consistently gave greater values for all four parameters, with 450 °C highest **Fig. 12(a-d)**, and the significance letters confirmed significant differences among the treatments.

Discussion

Pyrolysis temperature had a pronounced influence on the physicochemical and structural characteristics of the RHB. As the temperature increased from 250°C to 450°C, noticeable changes in biochar properties indicated a progressive thermal transformation of the biomass, which is expected to influence surface morphology, pore development, structural stability, and mineral availability[36]. Before pyrolysis, raw rice husk was characterized for its baseline properties, as shown in **Table 1.** Chemical properties of RHB at various pyrolysis temperature as shown in **Table 2.** By covering rice husks with aluminium foil in a crucible, the material was pyrolyzed in a muffle furnace for 2 hours at 250°C, 350°C, and 450°C. Through this process, the colour of the raw material changed from light brown to a dark, rich carbon material. After being allowed to cool for 24 hours as shown in **Fig. 2**, the biochar was then analyzed and used for an experiment with wheat[37].

The **Fig. 3** Biochar yield decreased with increasing pyrolysis temperature. The fitted regression analysis showed a negative trend, with an R^2 value of 0.8897. However, because the analysis was based on only three temperature levels, the strength and statistical significance of this relationship should be interpreted cautiously. The large drop in biochar yield from 250 to 350°C indicates a strong devolatilization phase during which hemicellulose and cellulose lose moisture, volatile substances, and light organic vapors. Lower temperatures increase biochar output, while higher temperatures intensify devolatilization, thereby decreasing biochar output[38,39]. The small difference in biochar output upon increasing the temperature from 350 to 450°C indicates that solid biochar was substantially altered at 300°C, and that almost all of the mass loss is due to inelastic decomposition of lignin[40].

Proximate analysis supports this observation **Fig. 4**. With rising temperature, moisture content declined as free and bound water were released **Fig. 4(a)**[41,42], while ash content increased owing to the loss of organic matter and retention of thermally stable minerals, notably silica in rice husk **Fig. 4(b)**[43]. Unlike the decrease commonly reported, volatile matter rose with temperature **Fig. 4(c)**, likely reflecting feedstock characteristics, pyrolysis conditions, residence time, and the analytical method[44,45]. Fixed carbon also increased **Fig. 4(d)**, indicating progressive carbonization into a stable, carbon-rich matrix and more efficient thermal conversion[46,47,48].

The SEM images and corresponding GL intensity maps revealed temperature-dependent changes in the surface morphology of RHB **Fig. 5(a–f).** At 250°C, the surface appeared rough and irregular, with poorly developed pores **Fig. 5(a, d),** suggesting limited structural transformation during pyrolysis. At 350°C, structural disruption and distinct pore openings became evident **Fig. 5(b, e)**. At 450°C, changes in pore morphology and exposed internal structures were observed **Fig. 5(c, f)**. These observations indicate that pore development did not follow a consistent increase with increasing pyrolysis temperature. Such variations may be associated with temperature-dependent thermal decomposition and devolatilization of lignocellulosic components, which can alter the structure and exposure of pre-existing voids, consistent with earlier reports on RHB [49,50]. The observed porous architecture may facilitate interactions between the biochar surface, water, and nutrients; however, SEM images alone cannot quantify specific surface area or pore volume, and these potential functional implications should be interpreted alongside complementary characterization results. Overall, pyrolysis temperature modified the surface morphology and pore characteristics of RHB.

EDAX analysis **Fig. 6(a–f)** showed that RHB produced at all three temperatures contained C, O, and Si in varying relative proportions, with the persistent Si and O signals confirming retention of the naturally silica-rich mineral fraction after pyrolysis[51,52,53]. At 250°C, the compact, irregular surface with blister-like features showed a prominent Si signal and relatively low C **Fig. 6(a, d)**[54], whereas at 350 °C, the more angular morphology exhibited a stronger C signal, indicating a surface dominated by the carbonaceous matrix **Fig. 6(b, e)**[55]. At 450 °C, the highly porous surface bearing angular char and mineral fragments still showed C, O, and Si **Fig. 6(c, f)**, indicating that silica remained stable while the rice husk matrix underwent progressive structural alteration[56]. As EDAX provides semi-quantitative, surface-sensitive data, these results reflect surface compositional trends rather than bulk composition[57].

The XRD patterns **Fig. 7(a–c)** exhibited broad diffraction backgrounds with superimposed features, suggesting the presence of disordered components and potentially crystalline mineral phases. At 250°C, the pattern showed a broad background with relatively weak diffraction features **Fig. 7(a)**[58,59]. At 350°C, some diffraction features became more distinguishable against the broad background **Fig. 7(b)**[60], while the 450°C sample also exhibited discernible diffraction features **Fig. 7(c)**[61]. However, these differences alone were insufficient to confirm an increase in the structural ordering of the carbonaceous matrix or silica-containing mineral fraction with increasing pyrolysis temperature. Consistent with the EDAX results, which detected Si and O alongside C in all samples, the findings support the retention of silicon- and oxygen-containing inorganic constituents in the RHB. Nevertheless,

the XRD patterns did not provide conclusive evidence of specific crystalline silica phases or increased silica structural ordering with increasing pyrolysis temperature.

Early, uniform germination is essential for crop establishment, allowing seedlings to exploit favourable conditions before stress or nutrient limitations arise[62]. RHB from all three pyrolysis temperatures significantly enhanced wheat germination relative to the control **Fig. (8)**, although treatment differences should be interpreted alongside the inherent germination traits of the wheat variety used[63]. The highest germination occurred with 450°C RHB **Fig. 8(d)**, likely owing to its well-developed surface pores and cavities (SEM), which may improve water retention and interaction with the growth medium[64], thereby supporting seed imbibition and radicle emergence.

As shown in **Fig. 9(a)**, the representative wheat seedlings exhibited visible differences in shoot and root growth among the control and RHB treatments produced at different pyrolysis temperatures (250, 350 and 450 °C). The seedlings treated with biochar produced at higher pyrolysis temperatures generally showed improved shoot and root development compared with the control. As illustrated in **Fig. 9(b)**, germination percentage increased progressively from 85% in the control to 87%, 91% and 95% under biochar treatments produced at 250, 350 and 450 °C, respectively[65]. Shoot length, root length and total seedling length also showed an increasing trend across the treatments, with the highest values observed at 450 °C. The root-to-shoot ratio showed comparatively smaller changes[66]. The reported *p*-values indicate statistically significant differences for the corresponding comparisons ($p < 0.05$). Overall, these findings suggest that RHB produced at 450 °C supported better wheat seedling establishment and early growth than the control and biochar produced at lower temperatures.

As shown in **Fig. 10**, wheat plants exhibited variations in overall growth, tillering and spike development under the control and RHB treatments produced at different pyrolysis temperatures. Compared with the control **Fig. 10(a)**, biochar-treated plants **Fig. 10 (b–d)** showed visible differences in plant growth and reproductive development. The plants treated with biochar produced at 350 and 450 °C appeared to exhibit differences in tiller and spike formation compared with those treated at 250 °C. These observations suggest that the pyrolysis temperature of RHB may influence wheat growth and reproductive development under pot conditions.

Wheat treated with 450 °C RHB showed significantly better growth than the control and other treatments for most parameters **Fig. 11**, consistent with biochar-enhanced soil nutrient availability[67]. Together with improved soil moisture and root penetration, these effects explain the greater plant height **Fig. 11(a)** and leaf number **Fig. 11(b)**, as adequate nitrogen and water support shoot elongation and leaf development[68,69]. The higher dry matter yield **Fig. 11(c)** reflects these improved growth conditions[82], although biochar performance also depends on its chemical composition, pH, ash content, surface functional groups, and soil type[70,71]. Likewise, the higher LAI **Fig. 11(d)** indicates improved nutritional and physiological status, as greater nitrogen availability promotes chlorophyll formation and photosynthesis, thereby enhancing assimilate production and biomass accumulation[72,73,74].

Biochar significantly improved wheat yield attributes, with the highest values under 450 °C RHB **Fig. 12**. The greater number of spikes per plant **Fig. 12(a)** likely reflects improved soil organic carbon, nutrient retention, and rhizosphere conditions that supported tiller survival

and their conversion into productive spikes[75,76]. Similarly, the higher number of spikelets per spike **Fig. 12(b)** suggests improved nutrient and water availability during spike differentiation, favouring the establishment of reproductive structures[77,78,79]. Consequently, grain yield per pot was highest under 450 °C biochar **Fig. 12(c)**, reflecting cumulative gains in yield components and soil nutrient dynamics; this agrees with global evidence that biochar increases long-term crop yields by about 16%, with stronger responses in wheat, closely linked to soil organic carbon[80,81]. Straw yield was also enhanced **Fig. 12(d)**, indicating greater vegetative biomass accumulation sustained by improved nutrient availability and soil conditions throughout growth[82].

Materials and Methods

Materials collection and preparation

Rice husk used as the feedstock for biochar production was collected from a local rice milling facility in Tenkasi district, Tamil Nadu, India. The samples were thoroughly cleaned to remove residual dirt, sand, and other extraneous impurities. The raw materials were then air-dried in the shade to reduce the initial moisture content; the biomass was then oven-dried at 65°C for 3 h to a constant weight, with moisture loss kept below 0.5%.

Rice husk material characterization

Prior to pyrolysis, the raw biomass feedstock was characterized for its chemical composition, as summarized in **Table 1**. Following pyrolysis, all samples were manually ground using an agate mortar and pestle to a particle size of less than 0.5 mm.

Biochar preparation

The slow pyrolysis of the dried rice husk sample was carried out in a laboratory muffle furnace at three temperatures (250, 350, and 450 °C) for a residence time of 2 hrs. The chosen pyrolysis temperatures were used to determine how thermal treatment has affected the physicochemical characteristics of RHB. The pyrolysis was carried out under oxygen-limited conditions to ensure thermal decomposition without complete combustion of the biomass. When the pyrolysis was complete, the laboratory oven was left to cool, and the resulting biochar was collected. The samples were ground into a fine powder, sieved through a 0.5 mm mesh, and stored in airtight containers for subsequent physicochemical characterization. All analyses were performed in triplicate. The overall process is shown in **Fig. 2.**

Biochar chemical properties

The pH and electrical conductivity (EC) of the biochar were determined in a 1:5 (w/v) biochar-to-deionized water suspension, which was shaken for 30 min, using a glass electrode and a conductivity meter, respectively[83]. Organic matter (OM) content was estimated by the loss-on-ignition method at 550 °C for 8 h, following the Test Methods for the Examination of Composting and Compost[84]**.** Total carbon (T-C), total nitrogen (T-N) and total hydrogen (T-H) contents of the RHB were determined using an elemental analyzer (TruSpec Micro, LECO, Michigan, USA). Calcium (Ca) and magnesium (Mg) contents were measured using a flame

photometer (PFP7, Jenway, UK). Silicon (Si) was extracted by nitric acid–hydrofluoric acid digestion and quantified by inductively coupled plasma optical emission spectrometry (ICP-OES; Plasma Quant PQ9000, Analytik Jena, Germany)[85] The chemical properties of the biochar are summarized in **Table 2.**

Yield of biochar

Biochar yield is influenced by the pyrolysis temperature. As the pyrolysis temperature increases, the biomass undergoes greater thermal decomposition via dehydration, devolatilization, and gasification, resulting in a reduction in biochar yield. Consequently, lower pyrolysis temperatures generally produce a higher biochar yield than higher temperatures. [86]the yield of biochar can be calculated using equation (2).

$$\text{Yield of the biochar (\%)} = \frac{\text{Mass of Biochar}}{\text{Mass of the raw materials}} \times 100 \quad (2)$$

Proximate analysis

Using proximate analysis, the ash, moisture, volatile matter, and fixed carbon contents were assessed.

Ash content was determined by placing approximately 1 g of oven-dried biochar in a pre-weighed ceramic crucible and heating it at 750 °C for 6 h in a muffle furnace. [87]the crucible was allowed to cool to room temperature, and the residual ash was weighed to determine the ash content (%) using the following equation (3)

$$\text{Ash (\%)} = \frac{\text{mass of residue after heating to 750}}{\text{initial mass of biochar}} \times 100 \quad (3)$$

Moisture content was determined by drying approximately 1 gm of air-dried biochar in a hot-air oven at 105 °C for 2 h. After cooling to room temperature, the samples were weighed, and the moisture content (%) was calculated using the following equation (4)[88].

$$\text{Moisture (\%)} = \frac{(\text{mass of air dried sample} - \text{mass of sample after drying at105 °C}}{\text{mass of air dried sample}} \times 100 \quad (4)$$

To ascertain the volatile components of the biochar, 1 g of oven-dried biochar was accurately weighed and burned at 750 °C for 11 min, and the mass loss was calculated using the following equation (5)[89].

$$\text{Volatile matter (\%)} = \frac{\text{oven dried sample mass} - \text{sample mass after heating to 750 °C}}{\text{mass of oven dried sample}} \times 100 \quad (5)$$

The fixed carbon content of the biochar was determined by difference from measured values of moisture, ash, and volatile matter. The fixed carbon content (%) was calculated using the following equation (6)

$$\text{Fixed carbon (\%)} = 100 - \left(\text{moisture content (\%)} + \text{ash (\%)} + \text{volatile matter (\%)}\right) \quad (6)$$

Characterization of biochar

SEM

The surface morphology and elemental composition of the RHB were characterized using a scanning electron microscope (SEM; CARL ZEISS EVO 18) equipped with an energy-dispersive X-ray spectroscopy (EDX) detector. Prior to analysis, the biochar samples were coated with a thin platinum–gold layer to improve electrical conductivity and minimize surface charging. Micrographs were recorded at magnifications ranging from 50× to 15,000× to examine the surface texture and porous structure of the biochar.

XRD

The crystalline characteristics of the RHB samples were examined using a Bruker D8 Advance X-ray diffractometer over a 2θ range of 5–80°, using Cu radiation at 40 kV and 30 mA, with a step size of 0.1°.

Soil-less Petri Dish Rice Husk Biochar for Wheat Seed Germination

A soil-less Petri dish bioassay was conducted to evaluate the influence of rice-husk biochar produced at different pyrolysis temperatures on wheat seed germination and early root development. Wheat seeds (*Triticum aestivum* L.) were used as the test material. Four treatments were established based on biochar pyrolysis temperature: control (0 g biochar), 250°C, 350°C, and 450°C biochar. For each treatment, biochar was applied at a rate of 1.0 g per Petri dish. The control treatment received no biochar. Biochar was evenly distributed over a layer of filter paper placed inside sterile Petri dishes. An equal volume of deionized water was added to all Petri dishes to maintain comparable moisture conditions. Uniformly sized, healthy wheat seeds were placed on the moistened filter paper containing the respective biochar treatments. Each treatment was maintained under identical experimental conditions, and the Petri dishes were covered with lids and incubated in the dark at 25°C for 72 h. The germination (%) was calculated using the following equation (7)[90].

$$Germination\ percentage(\%) = \frac{the\ number\ of\ germinated\ seeds\ in 7th\ day}{total\ number\ of\ seeds\ for\ testing} \times 100 \quad (7)$$

Effect of Rice Husk Biochar Pyrolysis Temperature on Early Wheat Seedling Growth

The effect of RHB produced at different pyrolysis temperatures (250, 350 and 450 °C) on the early growth of wheat seedlings was evaluated at 15 days after sowing (DAS), using an untreated control for comparison. At 15 DAS, seedlings were carefully collected from each treatment to assess their early growth characteristics. Shoot length and root length were measured to evaluate shoot and root development, respectively. Total seedling length was calculated as the sum of shoot length and root length and followed by root to shoot ratio. These parameters were used to compare the effects of biochar pyrolysis temperature on wheat seed germination and early seedling growth. The root to shoot ration was calculated using the following equation (8)[91].

$$\frac{Root}{Shoot} Ratio = \frac{Average\ root\ length}{Average\ shoot\ length} \quad (8)$$

For seedling length was used this measurement Seedling length = the sum of shoot length and root length of a seed[91].

Experimental site and plant material

A pot experiment was conducted during the 2025–2026 *Rabi* season under controlled open-field ambient conditions at the North farm of Karunya Institute of Technology and Sciences, Coimbatore, Tamil Nadu, India, to evaluate the effect of RHB amendment on the growth and yield responses of wheat (*Triticum aestivum*) variety HW 3094. Wheat seeds were procured from the ICAR Wheat Research Station, Wellington, Ooty, and healthy, uniform, disease-free seeds were selected for the experiment.

Preparation of the pot experiment and biochar application

The soil used for the pot experiment was collected from the experimental field surface layer, air-dried, gently crushed, and passed through a 2-mm sieve to remove stones and plant residues. RHB was used as the organic amendment. The initial physicochemical characteristics of the soil used for the pot experiment were determined prior to biochar application, and the results are presented in **Table 3**. The biochar was thoroughly mixed with the soil before filling the pots to ensure uniform distribution throughout the growing medium. Plastic pots with a capacity of approximately 5 kg were used for the experiment. Each pot was filled with 4.0 kg of air-dried soil. RHB was incorporated at a rate of 5% (w/w) of the soil weight. Accordingly, 200 g of biochar was added to each pot containing 4.0 kg of soil. The required quantity of biochar was thoroughly mixed with the soil to obtain a homogeneous soil–biochar mixture before sowing.

Experimental design and crop management

The pots were arranged in a completely randomized design (CRD) with four different temperatures a) Control, b) 250, c) 350, and d) 450 °C RHB treatments, with three replications. The pots were periodically randomized during the experimental period to reduce positional effects under ambient conditions. Healthy seeds of the wheat variety were planted uniformly in each pot, and seedlings were grown under similar growing conditions. Irrigation was uniformly applied to all pots as required to maintain adequate soil moisture without waterlogging. Other crop management practices were also performed uniformly for all treatments.

Agronomic traits of wheat

The agronomic assessments were conducted at regular intervals to measure wheat growth and yield performance across different soil-modification treatments. Other parameters, such as plant height (cm), yield (g plant^{-1} dry matter), number of leaves per plant, and leaf area index (LAI), were measured to assess crop growth progression across treatments. Plant height was measured from the base of the plant to the tip of the longest leaf (or spike, at later stages) using a meter scale, while dry matter production was determined by oven-drying the plant samples at 65–70°C until a constant weight was achieved. At the time of harvest, yield and yield-attributing parameters, including the number of spikes per plant, number of spikelets per spike, grain yield g per pot, and stover yield g per pot, were recorded from each treatment to evaluate

the influence of RHB amendment on the overall productivity of wheat. All observations were recorded from tagged/randomly selected plants within each pot to minimize observational bias, and the mean values were subjected to statistical analysis.

Statistical analysis

All laboratory experiments were conducted in triplicate, and the results were expressed as mean ± standard error (SE). Statistical analyses of soil and plant performed using IBM SPSS Statistics version 26.0. One-way analysis of variance (ANOVA) was used to assess significant differences among the temperature treatments, followed by Fisher's Least Significant Difference (LSD) test at $P < 0.05$ (*). Graphical representations were prepared using Origin Pro 2022 and the ggplot2 package in R to visualize treatment effects.

Conclusion

This study showed that pyrolysis temperature strongly shapes the properties and agronomic value of rice husk biochar (RHB). As the temperature rose from 250 to 450 °C, biochar yield decreased from 69% to 40%, with most of the mass loss occurring between 250 and 350 °C during the main devolatilization phase. Higher temperatures reduced moisture content and increased ash and fixed carbon contents, indicating greater carbonization and the buildup of thermally stable minerals. SEM and grey-level mapping showed that pores became more open and better defined at higher temperatures. EDAX and XRD confirmed that the silica-rich mineral fraction of the husk was retained and became more structurally ordered as temperature increased. These changes carried through to wheat performance. RHB produced at 450 °C gave the most vigorous seedlings, with longer shoots and better-developed roots. It also gave the greatest plant height (86.59 cm), leaf number, dry matter production, and leaf area index (3.78). Compared with the control, it increased spikes per plant from 35 to 48 and spikelets per spike from 12 to 21. Grain yield rose by 75% (from 12 to 21 g pot^{-1}) and stover yield by 33% (from 24 to 32 g pot^{-1}). These gains are likely due to improved nutrient retention, moisture availability, and rhizosphere conditions provided by the more porous, carbon-rich biochar.

Overall, converting rice husk into RHB at about 450 °C offers a practical way to reduce residue burning and improve wheat productivity. Multi-season field trials across different soils and application rates, along with direct measurements of surface area, nutrient release, and soil biological responses, are needed before wider recommendations can be made.

Acknowledgments: The authors are grateful to SAS, KITS, and ICAR-Wheat Research Station for providing the necessary research support and facilities.

Author contributions MSA: Writing original draft, data analysis, reviewing, editing, methodology and Supervision, and AR*: Writing original draft, reviewing, editing, conceptualizing, and SA: Reviewing, editing, and VV: Conceptualizing, supervision, reviewing, editing, and RK: Supervision, reviewing, editing, and PK: Investigation and reviewing, editing, and IP: Conceptualizing, methodology, reviewing, editing.

Funding: The work did not receive any specific grants from funding agencies in the commercial, public, or nonprofit sectors.

Data availability: The data that support the findings of this study are available from the corresponding author upon reasonable request.

Declarations

Competing interests: The authors declare no competing interests.

Table 1. Characterization properties of raw materials used in the production of biochar.

Characterized Parameters: Rice Husk Biomass	
Chemical Properties	
pH	6.5
Electrical conductivity (dS m^{-1})	1.20
Total organic matter (%)	77.06
Total organic carbon (%)	44.74
Total nitrogen (%)	0.49
Total phosphorus (%)	0.32
Total potassium (%)	0.56
Total calcium (%)	1.15
Total magnesium (%)	0.74
Total sodium (%)	0.16
Total sulphur (%)	0.04
C/N ratio	88:1
Physical Properties	
Moisture content (%)	10.57
Water holding capacity (g water g^{-1} dry)	1.5
Bulk density (kg m^{-3})	175
Porosity (%)	42.59

565 **Table 2.** Chemical properties of RHB produced at different pyrolysis temperatures (250, 350
566 and 450 °C). Values are mean ± standard error (n = 3). EC, electrical conductivity; OM, organic
567 matter; T-N, total nitrogen; T-C, total carbon; T-H, total hydrogen; T-Ca, total calcium; T-Mg,
568 total magnesium; T-Si, total silicon.

Biochar	**Temp**	**Chemical Properties Rice Husk Biochar**								
Type		**pH**	**EC (dsm^{-1})**	**OM (%)**	**T- N (%)**	**T- C (%)**	**T- H (%)**	**T- Ca ($g\ kg^{-1}$)**	**T- Mg ($g\ kg^{-1}$)**	**T- Si ($g\ kg^{-1}$)**
Rice Husk Biochar	250˚C	7.2 ± 0.2	1.28 ± 0.58	72 ± 5.48	0.8 ± 0.48	35.71 ± 3.89	5.47 ± 1.56	1.72 ± 1.39	1.12 ± 1.07	132.93 ± 3.50
	350˚C	7.9 ± 0.2	1.91 ± 0.39	65 ± 3.82	0.5 ± 0.03	42.9 ± 5.39	5.01 ± 1.89	1.93 ± 1.29	1.53 ± 1.18	155.84 ± 5.83
	450˚C	8.2 ± 0.1	2.10 ± 0.75	57 ± 2.17	0.3 ± 0.09	53.56 ± 4.29	4.62 ± 1.49	2.16 ± 1.69	1.68 ± 1.39	174.39 ± 2.49

569

570 **Table 3.** Physicochemical characteristics of the experimental soil used for the pot experiment

Characterized parameters of soil		
Chemical analysis		
Organic carbon (%)	0.55	Walkley and Black (1934)
Available nitrogen ($kg\ ha^{-1}$)	242.6	Subbiah and Asija (1956)
Available phosphorus ($kg\ ha^{-1}$)	13.2	Olsen *et al*. (1954)
Available potassium ($kg\ ha^{-1}$)	287.5	Stanford and English (1949)
pH	8.2	Jackson (1973)
EC ($dS\ m^{-1}$)	0.35	
Physical analysis		
Coarse Sand (%)	20.9	Gupta and Dakshinamoorthy (1981)
Fine Sand (%)	20.85	
Silt (%)	15.6	
Clay (%)	42.65	
Texture	Clay	
Bulk density ($Mg\ m^{-3}$)	1.4	

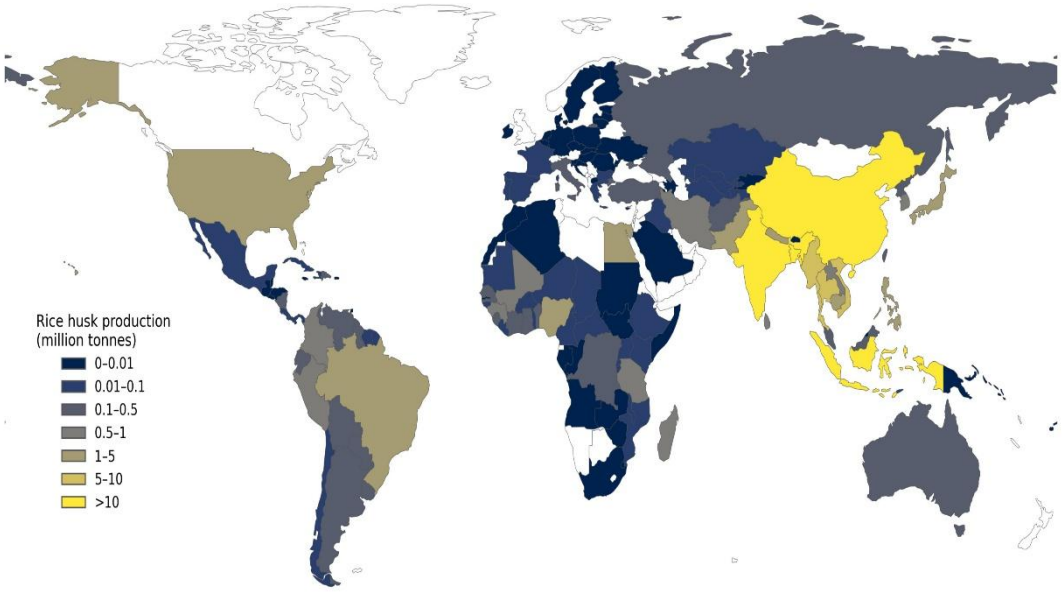

Figure. 1. Estimated rice husk production by country (million tonnes per year, Mt yr^{-1}). Husk was calculated as 20% of national paddy production (FAOSTAT, mean of 2022–2024). Global production was about 160 Mt yr^{-1}, with China (41.5 Mt) and India (41.3 Mt) contributing the most. White areas indicate no reported data.

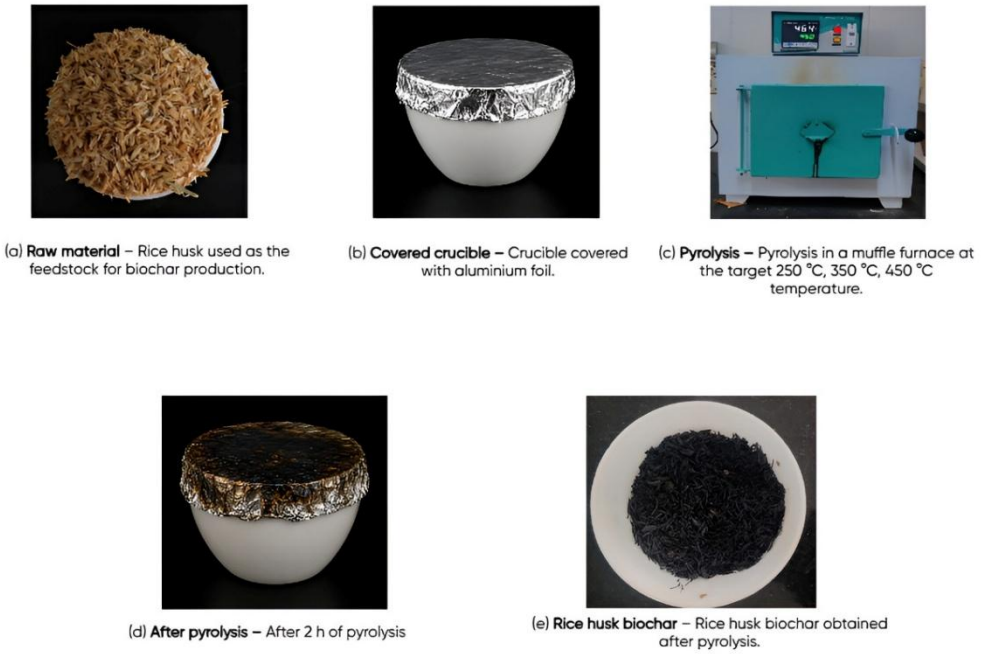

571 **Figure. 2.** Preparation and Production of Rice Husk Biochar at Different Pyrolysis
572 Temperatures

573

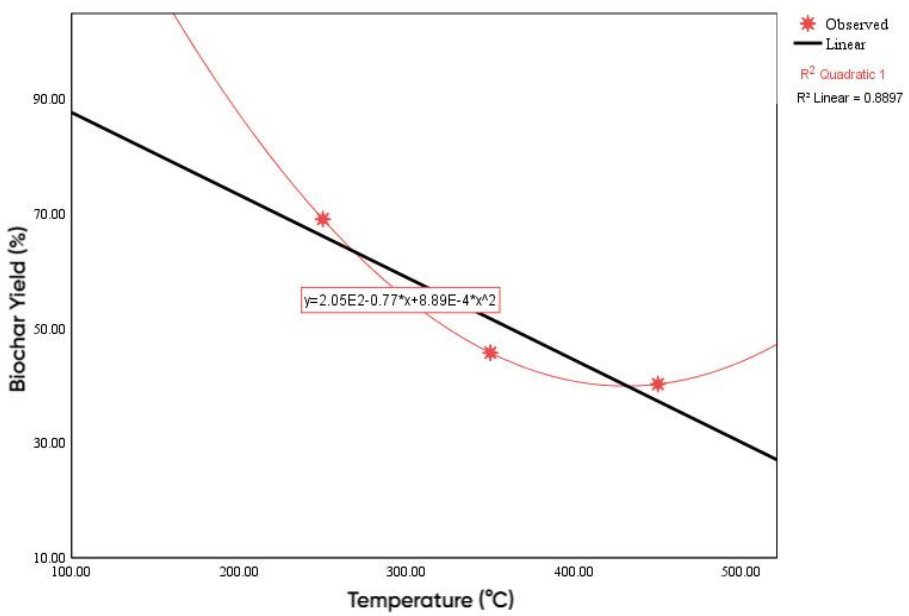

Figure. 3. Effect of pyrolysis temperature on biochar yield (%). The relationship between pyrolysis temperature and biochar yield was evaluated using linear and quadratic regression models. The observed biochar yield values are presented alongside the fitted regression curves, illustrating the decrease in biochar yield with increasing pyrolysis temperature.

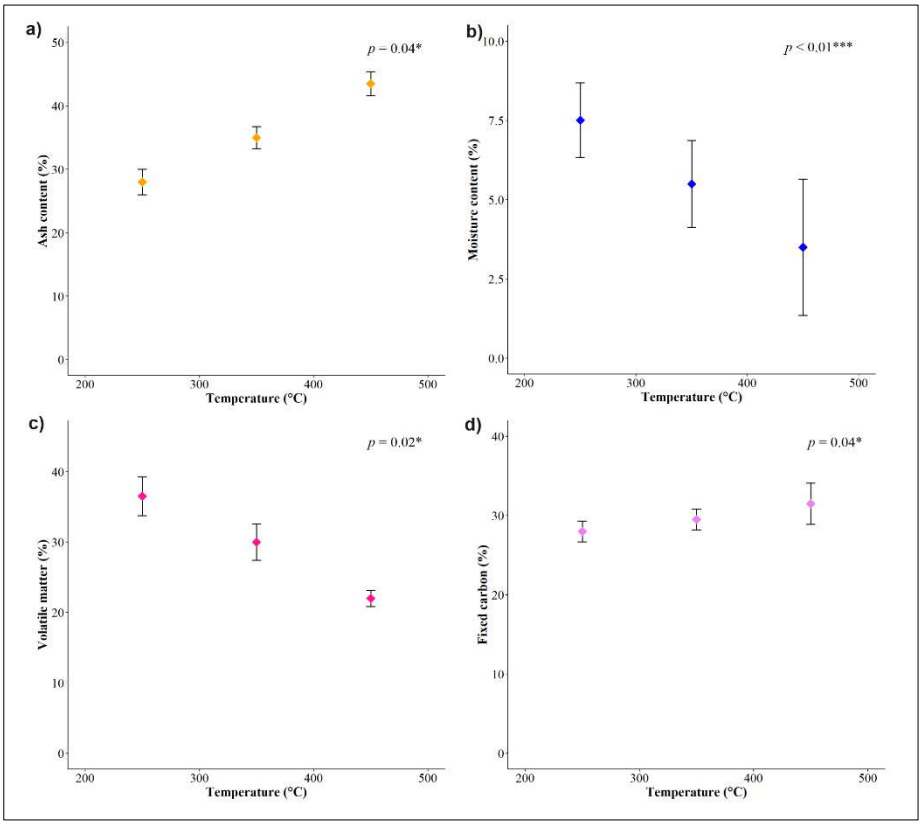

Figure 4. Effect of pyrolysis temperature on the proximate composition of rice husk biochar: (a) ash content, (b) moisture content, (c) volatile matter and (d) fixed carbon at 250, 350 and 450 °C. Points represent means ± SE (n = 3). Statistical significance is indicated as $p < 0.05$ (*) *and* $p < 0.001$ (***).

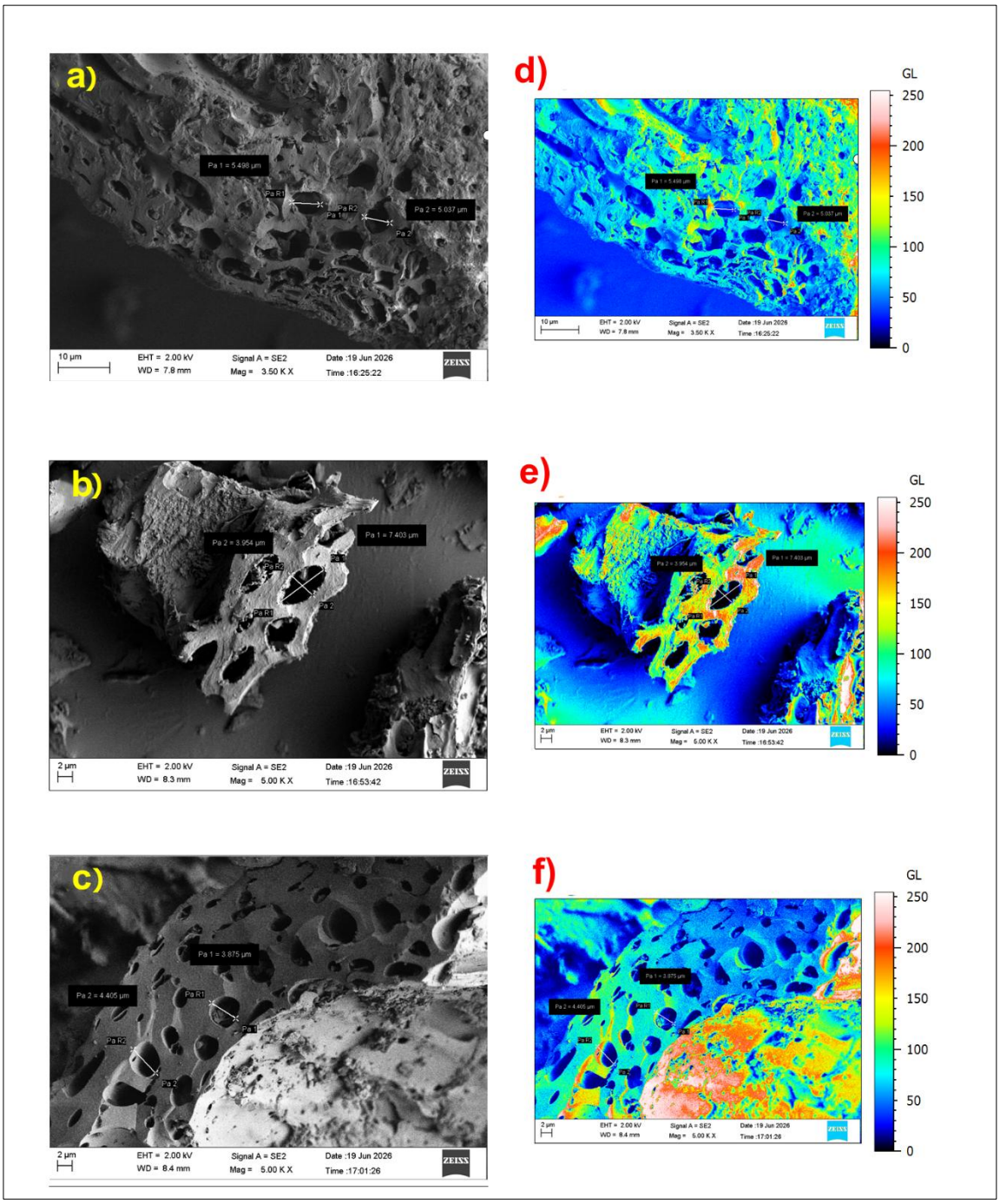

Figure 5. Scanning Electron Microscope (SEM) micrographs (a–c 250˚C, 350˚C and 450˚C) and their corresponding Grey Level (GL) intensity maps (d–f) illustrating the surface morphology and pore architecture of rice husk biochar

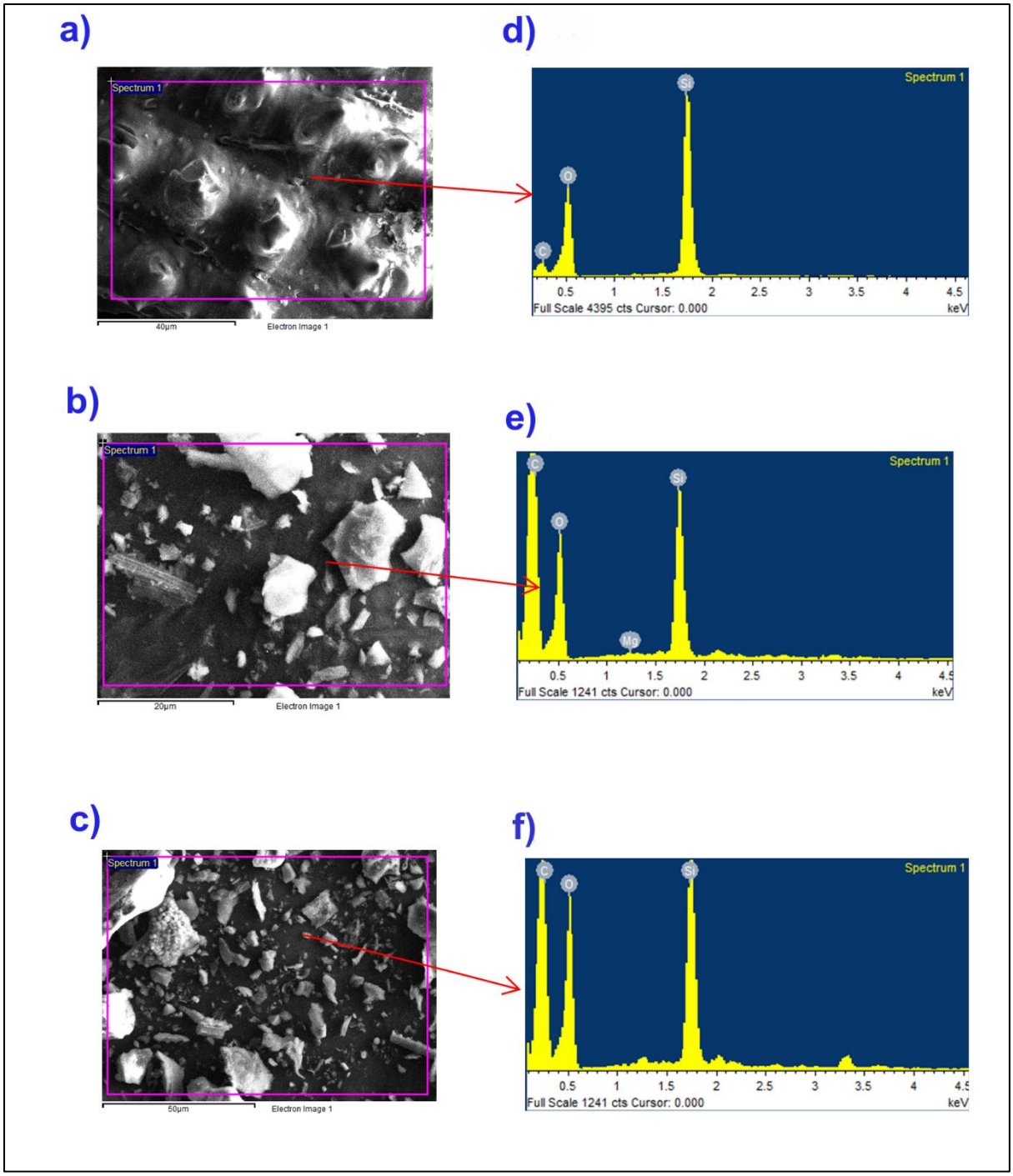

Figure 6. SEM micrographs of rice husk biochar produced at 250°C (a), 350°C (b), and 450°C (c), showing the selected EDAX analysis regions (Spectrum 1). The corresponding elemental spectra are presented in (d–f).

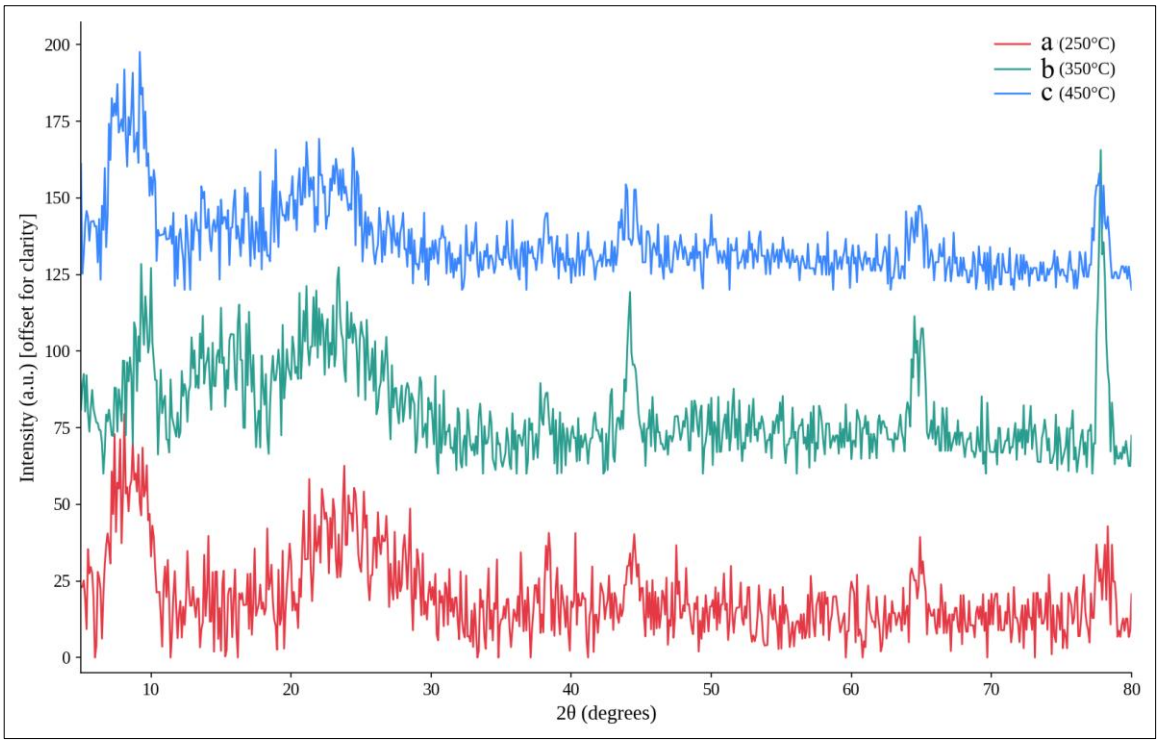

612 **Figure 7.** Comparative X-ray diffraction (XRD) patterns of rice husk biochar produced at
613 pyrolysis temperatures of 250°C (a), 350°C (b), and 450°C (c).

614

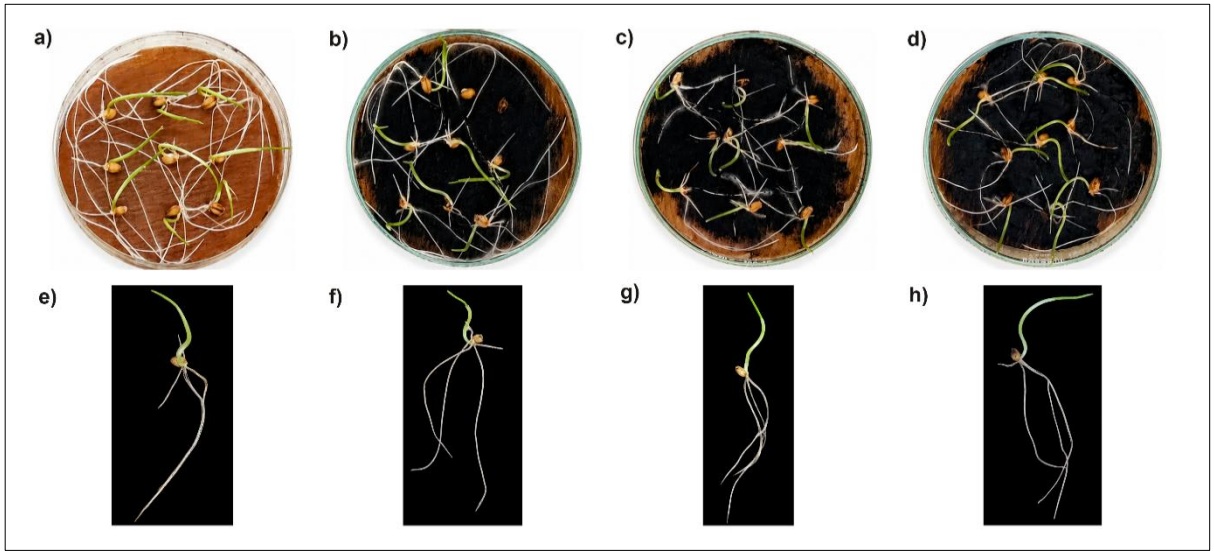

615 **Figure 8**. Influence of rice husk biochar produced at different pyrolysis temperatures on the
616 early growth and root development of wheat seedlings. (a–d) Representative images of
617 seedlings grown under the Control, 250°C, 350°C, and 450°C biochar treatments; (e–h)
618 Representative individual seedlings illustrating shoot and root growth under the corresponding
619 Control, 250°C, 350°C, and 450°C treatments, respectively.

620

621

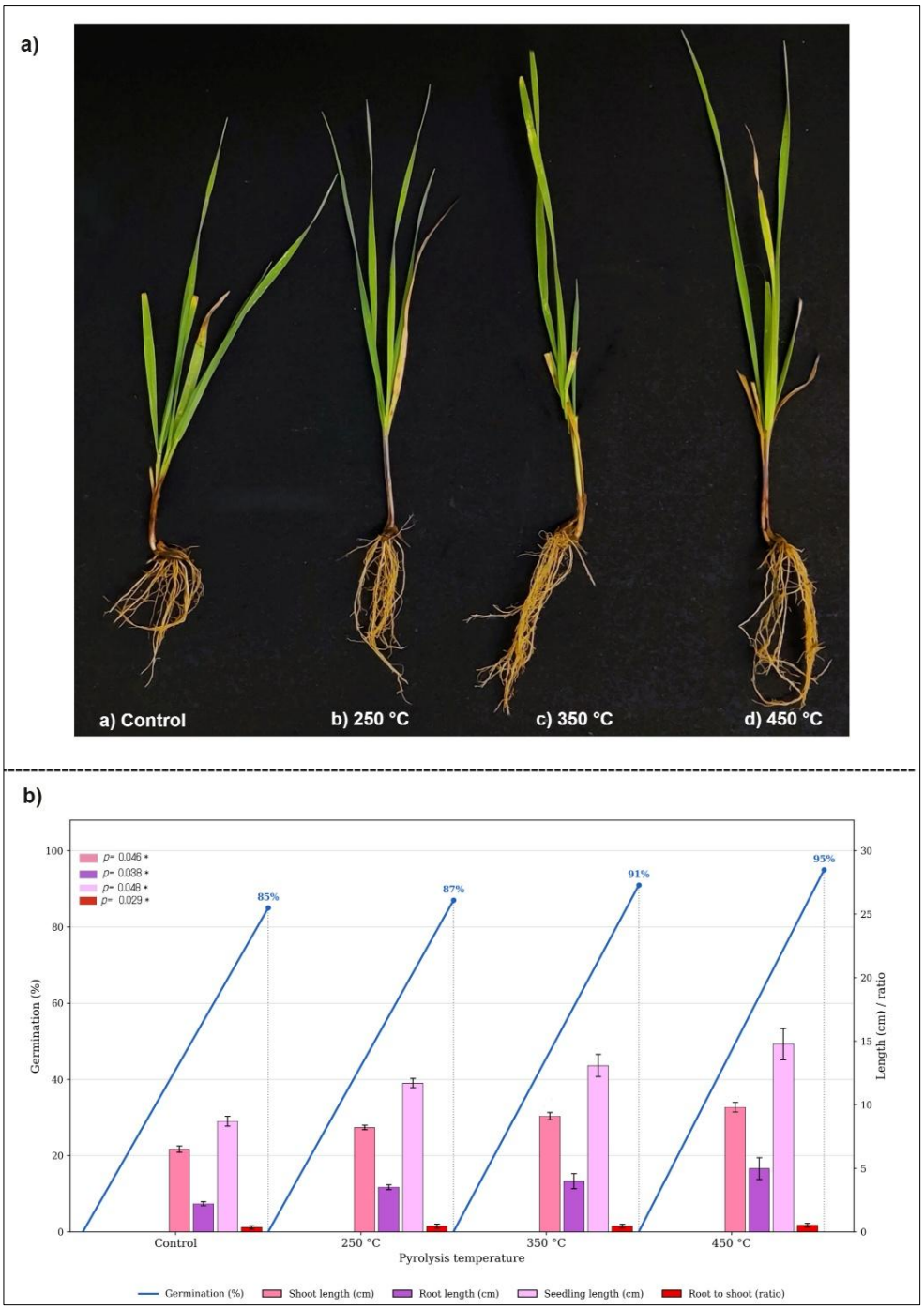

Figure 9. Effect of rice husk biochar pyrolysis temperature on seedling growth and germination performance. (a) Representative wheat seedlings under the control and rice husk biochar treatments produced at 250, 350 and 450 °C. (b) Germination percentage, shoot length, root length, seedling length and root-to-shoot ratio across the treatments. Bars represent mean values with error bars indicating variability among the treatments ± SE (n = 3). $p < 0.05$ (*) indicate the statistical significance of the respective comparisons.

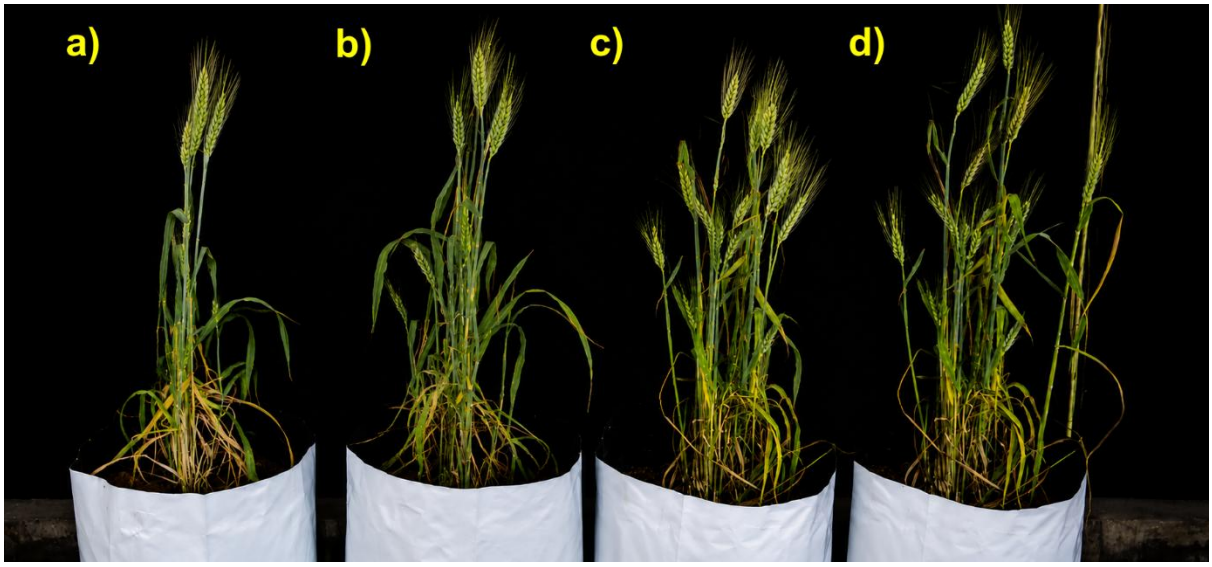

Figure 10. Comparative growth performance of wheat plants grown under control and rice husk biochar treatments produced at different pyrolysis temperatures. (a) Control, (b) 250°C biochar, (c) 350°C biochar, and (d) 450°C biochar treatments, showing the variation in plant growth, tillering, biomass development, and spike formation in response to temperature-derived rice husk biochar application under controlled pot conditions

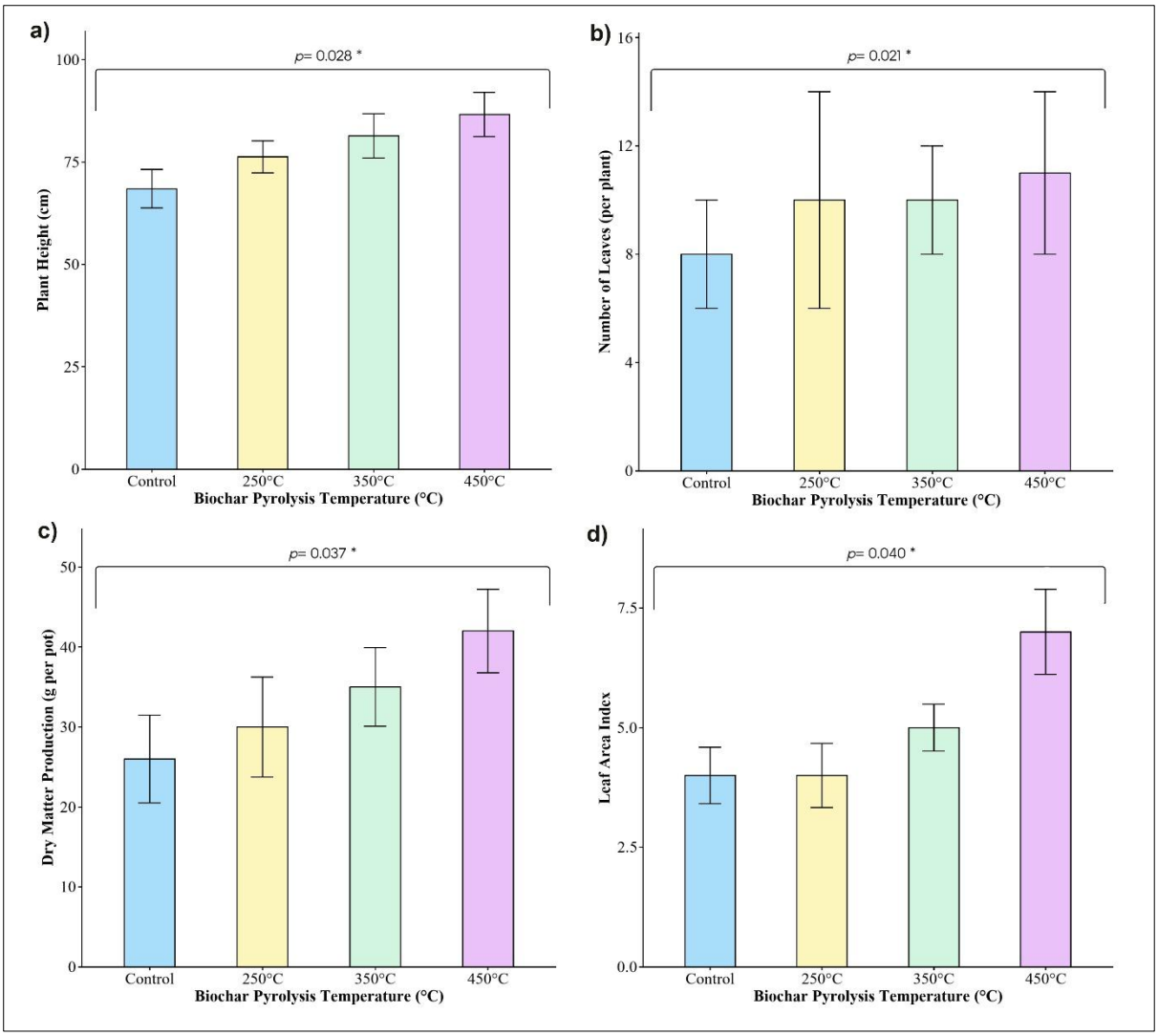

Figure 11. Effect of rice husk biochar produced at different pyrolysis temperatures on wheat growth parameters: a) plant height, b) number of leaves per plant, c) dry matter production, and d) leaf area index. Bars represent treatment means, and error bars indicate standard errors (SE) of the mean (n = 3). $p < 0.05$ (*) indicates a statistically significant difference between the treatments being compared.

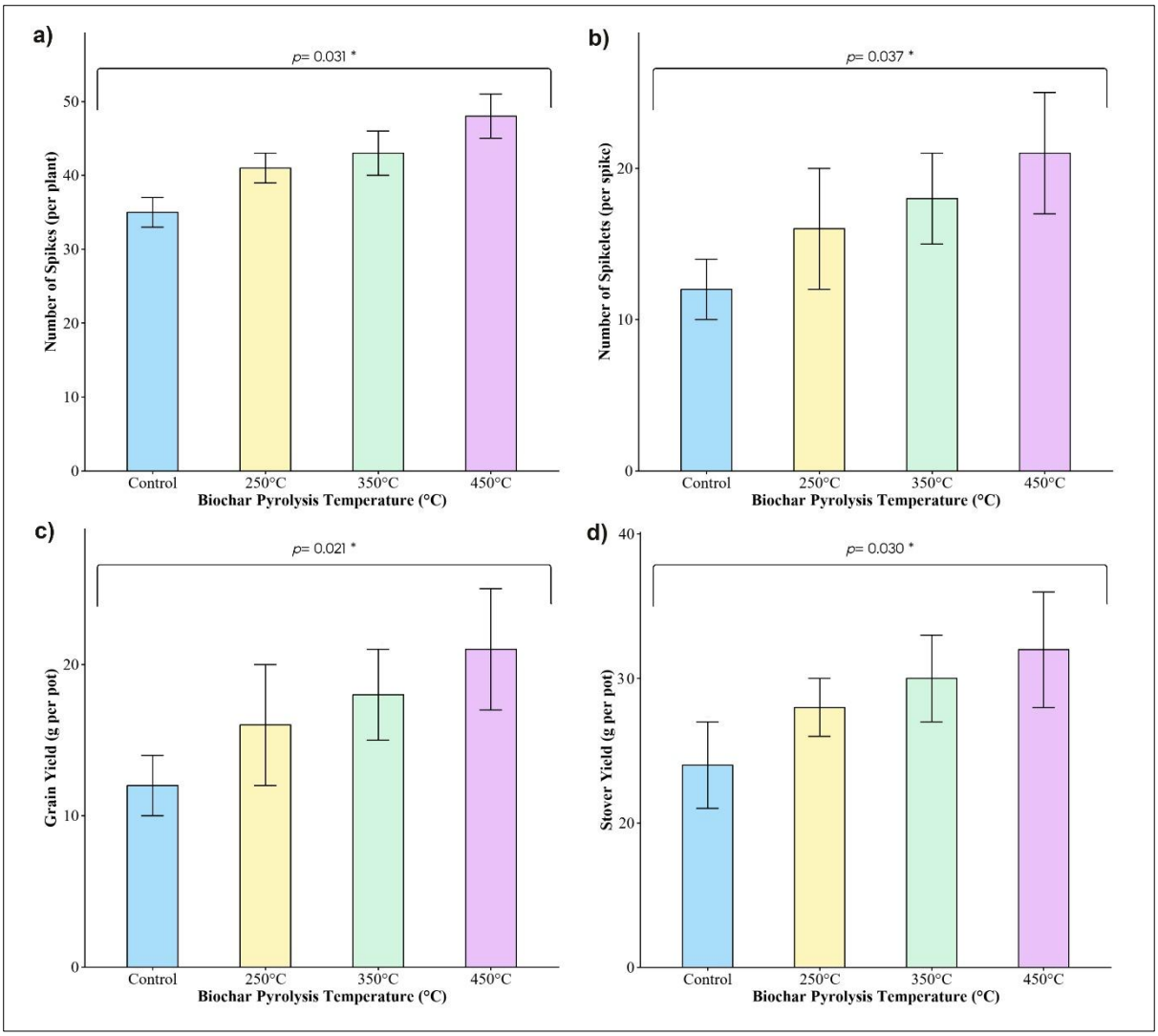

Figure 12. Effect of rice husk biochar produced at different pyrolysis temperatures on the yield attributes and yield of wheat: (a) number of spikes per plant, (b) number of spikelets per spike, (c) grain yield per pot, and (d) straw yield per pot. Bars represent treatment means, and error bars indicate standard errors (SE) of the mean (n = 3). $p < 0.05$ (*) indicates a statistically significant difference between the treatments being compared.

Reference:

1. Gupta, A. P., Upadhyay, P., Sen, T. & Dutta, J. Agricultural waste as a resource: the lesser travelled road to sustainability. In *Agriculture Waste Management and Bioresource: The Circular Economy Perspective* (eds Singh, S., Singh, P., Sharma, A. & Choudhury, M.) 1–20 (John Wiley & Sons, 2023). https://doi.org/10.1002/9781119808428.ch1
2. Verma, M., Singh, P. & Dhanorkar, M. Sustainability in residue management: a review with special reference to Indian agriculture. *Paddy Water Environ.* **22**(1), 1-15 https://doi.org/10.1007/s10333-023-00952-8 (2024).
3. Porichha, G. K., Hu, Y., Rao, K. T. V. & Xu, C. C. Crop residue management in India: Stubble burning vs. other utilizations including bioenergy. *Energies* **14**, 4281 (2021). https://doi.org/10.3390/en14144281
4. Parihar, D. S., Narang, M. K., Dogra, B., Prakash, A. & Mahadik, A. Rice residue burning in northern India: an assessment of environmental concerns and potential solutions–a review. *Environ. Res. Commun.* **5**(6), 062001 https://doi.org/10.1088/2515-7620/acb6d4 (2023).
5. Bhatt, R. Agricultural waste burning in northern India: Economic analysis and farmers' perspectives. Ph.D. dissertation, University of British Columbia (2020).
6. Nan, N., DeVallance, D. B., Xie, X. & Wang, J. The effect of bio-carbon addition on the electrical, mechanical, and thermal properties of polyvinyl alcohol/biochar composites. *J. Compos. Mater*. **50**, 1161–1168 https://doi.org/10.1177/0021998315589770 (2016).
7. DeVallance, D. B., Oporto, G. S. & Quigley, P. Investigation of hardwood biochar as a replacement for wood flour in wood polypropylene composites. *J. Elastomers Plast*. **48**, 510–522 https://doi.org/10.1177/0095244315589655 (2016).
8. Behazin, E., Misra, M. & Mohanty, A. K. Sustainable biocarbon from pyrolyzed perennial grasses and their effects on impact modified polypropylene biocomposites. *Compos. Part B Eng*. **118**, 116–124 https://doi.org/10.1016/j.compositesb.2017.03.003 (2017).
9. Shaik, D. S. et al. Impact of biomass burning on regional aerosol optical properties: a case study over northern India. *J. Environ. Manage*. **244**, 328–343 https://doi.org/10.1016/j.jenvman.2019.04.025 (2019).
10. Jain, R. & Naik, S. N. Sustainable management of agricultural waste in India. In *Handbook of Solid Waste Management: Sustainability through Circular Economy* (eds Baskar, C. et al.) 497–522 (Springer, Singapore, 2022).
11. Singh, J. et al. Environmental implications of rice and wheat stubble burning in north-western states of India. In *Advances in Health and Environment Safety* 47–55 (Springer, Singapore, 2018).
12. Singh, J. S. & Pandey, V. C. Fly ash application in nutrient poor agriculture soils: impact on methanotrophs population dynamics and paddy yields. *Ecotoxicol. Environ*. *Saf*. **89**, 43–51 https://doi.org/10.1016/j.ecoenv.2012.11.011 (2013).
13. Mekuria, W., Langan, S., Noble, A. & Johnston, R. Soil restoration after seven years of exclosure management in northwestern Ethiopia. *Land Degrad*. *Dev*. **28**, 1287–1297 https://doi.org/10.1002/ldr.2527 (2017)

14. Xu, X. et al. Indispensable role of biochar-inherent mineral constituents in its environmental applications: a review. *Bioresour. Technol*. **241**, 887–899 https://doi.org/10.1016/j.biortech.2017.06.023 (2017).
15. Agegnehu, G., Srivastava, A. & Bird, M. I. The role of biochar and biochar compost in improving soil quality and crop performance: a review. *Appl. Soil Ecol*. **119**, 156–170 https://doi.org/10.1016/j.apsoil.2017.06.008 (2017).
16. Kollah, B. et al. Interactive effect of biochar size and organic amendments on methane consumption in a tropical vertisol. *Soil Use Manag*. **31**, 52–59 https://doi.org/10.1111/sum.12168 (2015).
17. Zhang, H. Z., Chen, C. R., Gray, E. M. & Boyd, S. E. Effect of feedstock and pyrolysis temperature on properties of biochar governing end use efficacy. *Biomass Bioenergy* **105**, 136–146 https://doi.org/10.1016/j.biombioe.2017.06.024 (2017).
18. Kim, J. et al. Combined application of biochar and slow-release fertilizer reduces methane emission but enhances rice yield by different mechanisms. *Appl. Soil Ecol*. **118**, 57–62 https://doi.org/10.1016/j.apsoil.2017.05.006 (2017).
19. Luo, S. et al. Long-term biochar application influences soil microbial community and its potential roles in semiarid farmland. *Appl. Soil Ecol*. **117**, 10–15 https://doi.org/10.1016/j.apsoil.2017.04.024 (2017).
20. Rice Knowledge Bank. International Rice Research Institute. https://www.knowledgebank.irri.org/ (accessed 30 September 2023).
21. Elaigwu, S. E. & Greenway, G. M. Microwave-assisted hydrothermal carbonization of rapeseed husk: a strategy for improving its solid fuel properties. *Fuel Process. Technol*. **149**, 305–312 https://doi.org/10.1016/j.fuproc.2016.04.030 (2016).
22. Nizamuddin, S. *et al.* Synthesis and characterization of polylactide/rice husk hydrochar composite. *Sci. Rep.* **9**, 5445 https://doi.org/10.1038/s41598-019-41960-1 (2019).
23. Lin, L. et al. Dye adsorption of mesoporous activated carbons produced from NaOH-pretreated rice husks. *Bioresour. Technol.* **136,** 437-443 https://doi.org/10.1016/j.biortech.2013.03.048 (2013).
24. Runkle, B. R. et al. Socio-technical changes for sustainable rice production: rice husk amendment, conservation irrigation, and system changes. *Front. Agron.* **3,** 741557 https://doi.org/10.3389/fagro.2021.741557 (2021).
25. Gunal, E., Erdem, H. & Celik, I. Effects of three different biochars amendment on water retention of silty loam and loamy soils. *Agric. Water Manag.* **208,** 232–244 https://doi.org/10.1016/j.agwat.2018.06.004 (2018).
26. Xu, S. et al. Effect of biomass type and pyrolysis temperature on nitrogen in biochar, and the comparison with hydrochar. *Fuel* **291,** 120128 https://doi.org/10.1016/j.fuel.2021.120128 (2021).
27. Alkharabsheh, H. M. et al. Biochar and its broad impacts in soil quality and fertility, nutrient leaching and crop productivity: A review. *Agronomy* **11**(5), 993 https://doi.org/10.3390/agronomy11050993 (2021).
28. Burachevskaya, M. et al. Fabrication of biochar derived from different types of feedstocks as an efficient adsorbent for soil heavy metal removal. *Sci. Rep.* **13**(1), 2020 https://doi.org/10.1038/s41598-023-27638-9 (2023).
29. Cheng, C. H., Lehmann, J., Thies, J. E. & Burton, S. D. Stability of black carbon in soils across a climatic gradient. *J. Geophys. Res. Biogeosci.* **113**, G02027 https://doi.org/10.1029/2007JG000642 (2008).
30. Singh, B. P., Cowie, A. L. & Smernik, R. J. Biochar carbon stability in a clayey soil as a function of feedstock and pyrolysis tem perature. *Environ. Sci. Technol.* **46,** 11770–11778. https://doi.org/10.1021/es302545b (2012).

31. Pandey, M., Shrestha, J., Subedi, S. & Shah, K. K. Role of nutrients in wheat: A review. *Trop. Agrobiodivers.* **1**(1), 18-23 https://doi.org/10.26480/trab.01.2020.18.23 (2020).
32. Shah, S. S. et al. Impact of irrigation, fertilizer, and pesticide management practices on groundwater and soil health in the rice–wheat cropping system a comparison of conventional, resource conservation technologies and conservation agriculture. *Environ. Sci. Pollut. Res.* **32**(2), 533-558 https://doi.org/10.1007/s11356-024-35661-0 (2025).
33. Wang, M., Tafti, N. D., Wang, J. J. & Wang, X. Effect of pyrolysis temperature on Si release of alkali-enhanced Si-rich biochar and plant response. *Biochar* **3**(4), 469-484 https://doi.org/10.1007/s42773-021-00112-3 (2021).
34. Yuan, X., You, X., Wang, K. & Zhu, T. Tailored nanomaterials from urban lignocellulosic waste for soil and wastewater remediation: advancing towards sustainable environment. Nanotechnology **37**, 31 https://doi.org/10.1088/1361-6528/ae83bd (2026).
35. Luo, P. et al. Biochar-based fertilizers: advancements, applications, and future directions in sustainable agriculture—a review. *Agronomy* **15**(5), 1104 https://doi.org/10.3390/agronomy11050993 (2025).
36. Eduah, J. O., Henriksen, S. W., Nartey, E. K., Abekoe, M. K. & Andersen, M. N. Nonlinear sorption of phosphorus onto plant biomass-derived biochars at different pyrolysis temperatures. *Environ. Technol. Innov.* **19,** 100808 https://doi.org/10.1016/j.eti.2020.100808 (2020).
37. Hossain, T. Fabrication and characterization of rice husk pyrolyzed biochar reinforced polypropylene composite. M.Sc. thesis, Bangladesh University of Engineering and Technology, Dhaka, Bangladesh (2020).
38. Altıkat, A., Alma, M. H., Altıkat, A., Bilgili, M. E. & Altıkat, S. A comprehensive study of biochar yield and quality concerning pyrolysis conditions: A multifaceted approach. *Sustainability* **16**(2), 937 https://doi.org/10.3390/su16020937 (2024).
39. Avornyo, V. K. Increasing rice productivity in the lowland soils of the interior savanna of Ghana: the role of rice husk biochar and phosphate rock. Ph.D. thesis (Iowa State University, Ames, IA, USA, 2019).
40. Joseph, S. et al. How biochar works, and when it doesn't: A review of mechanisms controlling soil and plant responses to biochar. *GCB Bioenergy* **13**(11), 1731-1764 https://doi.org/10.1111/gcbb.12885 (2021).
41. Landa-Zavaleta, L. M. et al. Co-Pyrolysis of Urban Biosolids with rice Husk and Pruning Waste: effects on biochar quality, Stability and agricultural Applicability. *Eng* **7**(1), 32 https://doi.org/10.3390/eng7010032 (2026).
42. Tomczyk, A., Sokołowska, Z. & Boguta, P. Biochar physicochemical properties: pyrolysis temperature and feedstock kind effects. *Rev. Environ. Sci. Biotechnol.* **19**(1), 191-215 https://doi.org/10.1007/s11157-020-09523-3 (2020).
43. Thepjunthra, W., Vongphet, J., Puttrawutichai, S., Dechkrong, P. & Khawkomol, S. Characterization of Community-Scale Smokeless biochar production from Corncobs for potential soil Amendment and Climate-Smart agriculture. *Sustainability* **18**(14), 7177 https://doi.org/10.3390/su18147177 (2026).
44. Al-Ansari, T., Ismail, R., Mariyam, S. & Alherbawi, M. Valorising Waste Biomass into Activated Biochar Catalysts for Sewage Sludge Hydrothermal Liquefaction. Available at SSRN 7042888 http://dx.doi.org/10.2139/ssrn.7042888 (2026).
45. Wang, X. et al. Effect of pyrolysis upgrading temperature on particulate matter emissions from lignite semi-char combustion. *Energy Convers. Manage.* **195,** 384-391 https://doi.org/10.1016/j.enconman.2019.05.021 (2019).

46. Conti, R., Fabbri, D., Vassura, I. & Ferroni, L. Comparison of chemical and physical indices of thermal stability of biochars from different biomass by analytical pyrolysis and thermogravimetry. *J. Anal. Appl. Pyrolysis* **122,** 160-168 https://doi.org/10.1016/j.jaap.2016.10.003 (2016).
47. Crombie, K., Mašek, O., Sohi, S. P., Brownsort, P. & Cross, A. The effect of pyrolysis conditions on biochar stability as determined by three methods. *GCB Bioenergy* **5**(2), 122-131https://doi.org/10.1111/gcbb.12030 (2013).
48. Zhao, F. et al. The effect of temperature on pyrolysis products during oil shale thermal decomposition. *Sci. Rep.* **15**(1), 26135 https://doi.org/10.1038/s41598-025-11050-6 (2025).
49. Ikram, S., Das, O. & Bhattacharyya, D. A parametric study of mechanical and flammability properties of biochar reinforced polypropylene composites. Composites Part A: Applied Science and Manufacturing 91, 177–188 https://doi.org/10.1016/j.compositesa.2016.10.010 (2016)
50. Zhang, Q., Yi, W., Li, Z., Wang, L. & Cai, H. Mechanical Properties of Rice Husk Biochar Reinforced High Density Polyethylene Composites. Polymers 10, 286 https://doi.org/10.3390/polym10030286 (2018).
51. Abdullah, M., Baig, S., Martinez, M. P. H. & Sajjadi, B. Ultrasound-Induced Embedded-Silica Migration to biochar Surface: applications in agriculture and environmental sustainability. *Sustainability* **17**(23), 10813 https://doi.org/10.3390/su172310813 (2025).
52. Bhatt, M. et al. Co-pyrolysis of mixed municipal solid waste components in a semi-pilot scale rotary kiln: Synergistic effects on pyrolysis oil and biochar properties. *RSC Adv.* **16**, 35523–35545 (2026). https://doi.org/10.1039/D6RA02636B
53. Potyondy, D. O. The bonded-particle model as a tool for rock mechanics research and application: current trends and future directions. *Geosystem Engineering* **18**(1), 1-28 https://doi.org/10.1080/12269328.2014.998346 (2015).
54. Qudus, N. et al. Effect of Calcination temperature and Impregnation Time on Physicochemical and Textural properties of KOH-Modified rice Husk Ash Materials. *Journal of Composites Science* **10**(6), 290 https://doi.org/10.3390/jcs10060290 (2026).
55. Yapuchura, E. R., Tartaglia, R. S., Cunha, A. G., Freitas, J. C. & Emmerich, F. G. Observation of the transformation of silica phytoliths into SiC and SiO2 particles in biomass-derived carbons by using SEM/EDS, Raman spectroscopy, and XRD. *J. Mater. Sci.* **54**(5), 3761-3777 https://doi.org/10.1007/s10853-018-3130-6 (2019).
56. Sajjadi, B., Chen, W. Y. & Egiebor, N. O. A comprehensive review on physical activation of biochar for energy and environmental applications. *Reviews in Chemical Engineering* **35**(6), 735-776 https://doi.org/10.1515/revce-2017-0113 (2019).
57. Elashry, M. E., Khater, E. G. & Ali, S. A. Modeling and kinetic analysis of structural disintegration and biodegradation of biocomposite cultivating pots from agricultural waste. *Sci. Rep.* **15**(1), 43824 https://doi.org/10.1038/s41598-025-30302-z (2025).
58. Aliyu, A. S. et al. Synthesis and characterisation of rice husk and palm fruit bunch silica: compositional, structural, and thermal analyses. *Biomass Convers. Biorefin.* **15**(3), 3533-3544 https://doi.org/10.1007/s13399-024-05525-1 (2025).
59. Satbaev, B. et al. Rice husk research: from environmental pollutant to a promising source of organo-mineral raw materials. *Materials* **14**(15), 4119 https://doi.org/10.3390/ma14154119 (2021).
60. Biswas, B., Balla, P., Krishna, B. B., Adhikari, S. & Bhaskar, T. Physiochemical characteristics of bio-char derived from pyrolysis of rice straw under different

temperatures. *Biomass Convers. Biorefin.* **14**(12), 12775-12783 https://doi.org/10.1007/s13399-022-03261-y (2024).
61. Kusmardini, D., Budianto, B., Yasin, R. E. & Suparmi, A. Biological Pretreatment as a Precursor Strategy for Modulating Kinetic Behavior and Pyrolysis Product Distribution of Lignocellulosic Biomass. *Chem. Afr.* **9**(6), 288 https://doi.org/10.1007/s42250-026-01801-x (2026).
62. Reed RC, Bradford KJ, Khanday I. Seed germination and vigor: ensuring crop sustainability in a changing climate. *Heredity (Edinb)*. **128**(6):450–9. https://doi.org/10.1038/s41437-022-00497-2 (2022).
63. Worrall D, Holroyd GH, Moore JP, Glowacz M, Croft P, Taylor JE, et al. Treating seeds with activators of plant defence generates long-lasting priming of resistance to pests and pathogens. *New Phytol*. **193**(3):770–8. https://doi.org/10.1111/j.1469-8137.2011.03987 (2012).
64. Sembada, A. A. et al. Candle soot colloids enhance tomato (Solanum lycopersicum) seed germination and seedling quality. *Discov. Agric.* **2**(1), 1 https://doi.org/10.1007/s44279-024-00011-8 (2024).
65. Ighalo, J. O. et al. Biochar for ameliorating soil fertility and microbial diversity: From production to action of the black gold. *iScience* **28**, 111524 (2025). https://doi.org/10.1016/j.isci.2024.111524
66. orno, M. L., Eduah, J. O., Müller-Stöver, D. S. & Liu, F. Effect of different biochars on phosphorus (P) dynamics in the rhizosphere of *Zea mays* L. (maize). *Plant Soil* **431**(1), 257–272 (2018). https://doi.org/10.1007/s11104-018-3762-y
67. Yang, Y. et al. Elucidating the impact of biochar with different carbon/nitrogen ratios on soil biochemical properties and rhizosphere bacterial communities of flue-cured tobacco plants. *Front. Plant Sci.* **14,** 1250669 https://doi.org/10.3389/fpls.2023.1250669 (2023).
68. Guo, M., Song, W. & Tian, J. Biochar-facilitated soil remediation: mechanisms and efficacy variations. *Front. Environ. Sci*. **8**, 521512 https://doi.org/10.3389/fenvs.2020.521512 (2020).
69. Silva, L. G., de Andrade, C. A. & Bettiol, W. Biochar amendment increases soil microbial biomass and plant growth and suppresses Fusarium wilt in tomato. *Trop. Plant Pathol*. **45**, 73–83 https://doi.org/10.1007/s40858-020-00332-1 (2020).
70. Abukari, A., Kaba, J. S., Dawoe, E. & Abunyewa, A. A. A comprehensive review of the effects of biochar on soil physicochemical properties and crop productivity. *Waste Dispos. Sustain. Energy* **4**(4), 343-359 https://doi.org/10.1007/s42768-022-00114-2 (2022).
71. Jabborova, D. et al. Growth response of ginger (Zingiber officinale), its physiological properties and soil enzyme activities after biochar application under greenhouse conditions. *Horticulturae* **7**, 250 https://doi.org/10.3390/horticulturae7080250 (2021).
72. Aluko, O. O., Li, C., Wang, Q. & Liu, H. Sucrose utilization for improved crop yields: A review article. *Int. J. Mol. Sci.* **22**(9), 4704 https://doi.org/10.3390/ijms22094704 (2021).
73. Mae, T. Physiological nitrogen efficiency in rice: nitrogen utilization, photosynthesis, and yield potential. *Plant Soil* **196**(2), 201-210 https://doi.org/10.1023/A:1004293706242 (1997).
74. Man, J., Yu, Z. & Shi, Y. Radiation interception, chlorophyll fluorescence and senescence of flag leaves in winter wheat under supplemental irrigation. *Sci. Rep.* **7**(1), 7767 https://doi.org/10.1038/s41598-017-07414-2 (2017).

75. Khan, Z. et al. Engineered biochar improves nitrogen use efficiency via stabilizing soil water-stable macroaggregates and enhancing nitrogen transformation. *Biochar* **5**(1), 52 https://doi.org/10.1007/s42773-023-00252-8 (2023).
76. Tang, K. H. D. Biochar amendments for soil restoration: Impacts on nutrient dynamics and microbial activity. *Environments* **12**(11), 425 https://doi.org/10.3390/environments12110425 (2025).
77. Joseph, S. et al. How biochar works, and when it doesn't: A review of mechanisms controlling soil and plant responses to biochar. *GCB Bioenergy* **13**(11), 1731-1764 https://doi.org/10.1111/gcbb.12885 (2021).
78. Pandian, K., Vijayakumar, S., Mustaffa, M. R. A. F., Subramanian, P. & Chitraputhirapillai, S. Biochar–a sustainable soil conditioner for improving soil health, crop production and environment under changing climate: a review. *Front. Soil Sci.* **4,** 1376159 https://doi.org/10.3389/fsoil.2024.1376159 (2024).
79. Xu, P. et al. Research progress on effects of biochar on soil environment and crop nutrient absorption and utilization. *Sustainability* **15**(6), 4861 https://doi.org/10.3390/su15064861 (2023).
80. Foulkes, M. J. et al. Raising yield potential of wheat. III. Optimizing partitioning to grain while maintaining lodging resistance. *J. Exp. Bot.* **62**(2), 469-486 https://doi:10.1093/jxb/erq300 (2011).
81. Sinha, P., Marchuk, S., Harris, P., Antille, D. L. & McCabe, B. K. Land application of biosolids-derived biochar in Australia: a review. *Sustainability* **15**(14), 10909 https://doi.org/10.3390/su151410909 (2023).
82. Chen, L. et al. Effects of straw return and straw biochar on soil properties and crop growth: A review. *Front. Plant Sci.* **13,** 986763 https://doi.org/10.3389/fpls.2022.986763 (2022).
83. Abad, M., Noguera, P., Puchades, R., Maquieira, A. & Noguera, V. Physico-chemical and chemical properties of some coconut coir dusts for use as a peat substitute for containerised ornamental plants. *Bioresour. Technol*. **82**, 241–245 https://doi.org/10.1016/S0960-8524(01)00189-4 (2002).
84. TMECC, 2002.Test Methods for the Examination of Composting and Compost, USDA and US. Composting Council, Bethesda, MD.
85. Novozamsky, I., van Eck, R., Houba, V. J. G. & van der Lee, J. J. Solubilization of plant tissue with nitric acid–hydrofluoric acid–hydrogen peroxide in a closed-system microwave digestor. *Commun. Soil Sci. Plant Anal.* **27**, 867–875 (1996). https://doi.org/10.1080/00103629609369603
86. Sahoo, S. S., Vijay, V. K., Chandra, R. & Kumar, H. Production and characterization of biochar produced from slow pyrolysis of pigeon pea stalk and bamboo. *Cleaner Eng. Technol*. **3**, 100101 https://doi.org/10.1016/j.clet.2021.100101 (2021).
87. Ganesapillai, M. et al. Waste to energy: a review of biochar production with emphasis on mathematical modelling and its applications. *Heliyon* **9**, e14873 https://doi.org/10.1016/j.heliyon.2023.e14873 (2023).
88. ASAE Standards. ASAE S353 DEC97: Moisture Measurement—Meat and Meat Products, 45th ed. (American Society of Agricultural Engineers, St. Joseph, MI, 1998).
89. Dhar, S. A., Sakib, T. U. & Hilary, L. N. Effects of pyrolysis temperature on production and physicochemical characterization of biochar derived from coconut fiber biomass

through slow pyrolysis process. *Biomass Convers. Biorefin*. **12**, 2631–2647 https://doi.org/10.1007/s13399-020-01116-y (2022).

90. Ren, Y., Wang, W., He, J., Zhang, L., Wei, Y. & Yang, M. Nitric oxide alleviates salt stress in seed germination and early seedling growth of pakchoi (*Brassica chinensis* L.) by enhancing physiological and biochemical parameters. *Ecotoxicol. Environ. Saf.* **187**, 109785 (2020). https://doi.org/10.1016/j.ecoenv.2019.109785

91. Raskar, S. & Laware, S. L. Effect of titanium dioxide nanoparticles on seed germination and germination indices in onion. *Plant Sci. Feed* **3**, 103–107 (2013).